RSC Pharmaceutics

ROYAL SOCIETY OF CHEMISTRY

PAPER

View Article Online
View Journal | View Issue

Cite this: *RSC Pharm.*, 2025, **2**, 1514

Cyclodextrin-based nanosponge co-delivery of doxorubicin and EMD: synergistic anticancer activity with improved selectivity toward cancer cells

Sunisa Thongsom,[a] Paolo Di Gianvincenzo,[a] Giulia Ciattaglia,[b] Ahmed Subrati,[a] Desiré DiSilvio,[a] Ariadna M. Birocco,[c] Marco D'Abramo,[b] Chanchai Boonla,[d] Pithi Chanvorachote[e,f] and Sergio E. Moya *[a,d]

Combination therapy is a promising strategy in cancer treatment aiming at improving therapeutic efficacy and overcoming tumour resistance. Cyclodextrin-based nanosponges (EpCN) were developed here for the co-delivery of doxorubicin (DX), a hydrophilic chemotherapeutic agent, alongside *N*,*N*-bis (5-ethyl-2-hydroxybenzyl) methylamine (EMD), a hydrophobic compound targeting c-Myc. EpCNs were synthesized by crosslinking β-cyclodextrin with epichlorohydrin, then DX and EMD were loaded either separately or together into the nanosponge. The nanosponges were extensively characterized combining Dynamic Light Scattering (DLS), Atomic Force Microscopy (AFM), Scanning Electron Microscopy (SEM) and Nuclear Magnetic Resonance (NMR). The dual-loaded nanosponges with DX and EMD (DX/EMD-EpCN) displayed uniform sizes (30 ± 13 nm), high encapsulation efficiency (>98%), a zeta potential of +23 ± 4 mV, and a pH-responsive drug release, with faster release at acidic pH mimicking tumour conditions. *In vitro* studies were carried out on cancerous (A549 and MCF-7) and non-cancerous (WI-38) cells to explore the therapeutic potential of the drug-loaded EpCNs. Cytotoxicity results demonstrated that DX/EMD-EpCNs significantly reduced cell viability, more than free drugs or single drug-loaded EpCNs in both cancerous cell lines. The therapeutic potential of combining DX and EMD was improved by the encapsulation into EpCN, as indicated by a strong synergism (combination index: <0.6), with a reduced effective dose, and improved drug uptake in cancer cells while sparing normal cells. Cell cycle analysis reveals that DX/EMD-EpCNs induced multi-phase arrest at the G0/G1 and G2/M phases, leading to a superior apoptotic induction as confirmed by the annexin V/Zombie UV staining. Western blot analysis demonstrated that the DX/EMD-EpCN significantly suppressed c-Myc and Bcl-2 expression while increased cleaved-PARP expression in both cancer cell lines, indicating the activation of caspase-dependent apoptosis. In contrast, the downregulation of c-Myc and Bcl-2 by single drug-loaded EpCNs altered cell cycle progression but did not significantly induced apoptosis. The co-delivery of DX and EMD by EpCNs enhanced therapeutic potency through various mechanisms. These findings highlight the potential of cyclodextrin-based nanosponges as a versatile drug delivery platform for combination chemotherapy profiting from their capability of simultaneously encapsulating both hydrophilic and hydrophobic drugs.

Received 10th July 2025,
Accepted 25th August 2025

DOI: 10.1039/d5pm00183h

rsc.li/RSCPharma

1. Introduction

Cancer remains one of the leading causes of death worldwide.[1] Conventional chemotherapy kills rapid-dividing cancer cells by targeting DNA replication and mitosis, hence inhibiting tumour growth and preventing metastases.[2,3] Most chemotherapeutic drugs, however, have several disadvantages including low solubility, a short half-life in circulation, and non-selectivity that inevitably damages healthy cells leading to undesired side effects.[4–6] The combination therapy has become a promising approach to overcome these disadvantages, since it could

[a]*Soft Matter Nanotechnology Lab, CIC biomaGUNE, Paseo Miramón 182, 20014 Donostia-San Sebastián, Gipuzkoa, Spain. E-mail: smoya@cicbiomagune.es*
[b]*Chemistry Department, University of Rome "La Sapienza", P.le Aldo Moro 5, 00185 Rome, Italy*
[c]*Department of Biological Sciences, Faculty of Pharmacy and Biochemistry, University of Buenos Aires, Junin 956, C1113AAD Buenos Aires, Argentina*
[d]*Department of Biochemistry, Faculty of Medicine, Chulalongkorn University, Bangkok 10330, Thailand*
[e]*Department of Pharmacology and Physiology, Faculty of Pharmaceutical Sciences, Chulalongkorn University, Bangkok 10330, Thailand*
[f]*Center of Excellence in Cancer Cell and Molecular Biology, Faculty of Pharmaceutical Sciences, Chulalongkorn University, Bangkok 10330, Thailand*

provide synergistic benefits, enhance therapeutic efficacy, and reduce side effects. By simultaneously targeting multiple signalling pathways involved in tumour progression and survival, combination therapies can improve treatment outcomes and help circumvent mechanisms of drug resistance.[7]

Among the commonly used chemotherapeutic drugs, doxorubicin (DX) is frequently used for the treatment of many solid tumours, showing a strong anticancer action. DX intercalates into DNA, inhibiting topoisomerase II, and inducing apoptosis in rapidly proliferating cells. DX also induces apoptosis through an increase in reactive oxygen species production. However, its clinical use is often limited by dose-dependent cardiotoxicity and the development of resistance over time.[8] *N*,*N*-Bis (5-ethyl-2-hydroxybenzyl) methylamine (EMD) is a recently synthesized compound that targets the oncogenic transcription factor c-Myc.[9,10] The c-Myc protein is frequently overexpressed in various human cancers and associated with tumour aggressiveness, therapeutic resistance, and poor clinical outcomes.[11] EMD induces c-Myc degradation through a ubiquitin-proteasomal mechanism, hence drastically reducing its stability and expression, leading to the initiation of a caspase-dependent apoptosis cascade.[9] This c-Myc depletion alters the transcription of genes critical for cell survival, metabolism, and stress resistance, therefore sensitizing cancer cells to cytotoxic drugs and improving therapeutic efficacy.[12] Nevertheless, despite its therapeutic value, low bioavailability and poor water solubility drastically restrict the clinical usage of EMD.

Cyclodextrin-nanosponges (CNs) are versatile and effective drug carriers. CNs are intricate macromolecular structures formed by several crosslinked cyclodextrins (CDs) displaying nanochannels generated between cross-linked CD units, resulting in a three-dimensional network that can encapsulate a wide range of therapeutic molecules.[13] CNs offer several advantages, including a high capacity for drug loading, improved solubility in aqueous environments, regulated and prolonged drug release.[14] Their capability to encapsulate both hydrophilic and hydrophobic compounds makes them especially appealing for therapeutic combination strategy.[15] Our previous study demonstrated that CN encapsulation significantly improved the solubility and anticancer activity of EMD, which is a poorly water-soluble compound.[16]

In this study, we formulated cyclodextrin-based nanosponges for the dual encapsulation of DX and EMD, aiming at the delivery of a synergistically therapeutic effect in killing cancer cells. We hypothesized that EMD molecules were trapped in the hydrophobic sites of CNs while DX molecules were encapsulated in the CN's hydrophilic channels. We investigated whether these dual drugs-carrying CNs could enhance the overall anticancer efficacy in cancerous cell lines (A549 and MCF-7). Selectivity of these dual drug nanocarriers was also tested in non-cancerous cell line (WI-38). Our findings suggested that cyclodextrin-based nanosponges represented a novel effective system for dual-drug delivery profiting from CNs capacity to encapsulate both hydrophilic and hydrophobic drugs and emphasises the potential of CNs in the design of combination chemotherapy strategies to improve the therapeutic efficacy and help reduce an undesired off-target damage.

2. Materials and methods

2.1. Materials

Doxorubicin (DX), β-cyclodextrin (β-CD), epichlorohydrin (EP), sulphorhodamine B (SRB), trichloroacetic acid (TCA), RIPA lysis buffer, Triton X-100, and protease inhibitor cocktail were purchased from Sigma-Aldrich (St. Louis, MO, USA). *N*,*N*-Bis (5-ethyl-2-hydroxybenzyl) methylamine (EMD) was kindly provided by Assoc. Prof. Worawat Wattanathana (Kasetsart University, Bangkok, Thailand). Float-A-Lyzer®G2 dialysis tubes (3.5–5 kDa) were purchased from Repligen (former Spectrum Labs, Waltham, MA, USA). Pierce BCA Protein Assay Kits, annexin V Apoptosis Detection Kit FITC, phosphate buffered saline (PBS), and 4′,6-diamidino-2-phenylindole (DAPI) was purchased from Thermo Fisher Scientific (Waltham, MA, USA). Zombie UV Fixable Viability Kit was purchased from BioLegend (San Diego, CA, USA). Polyvinylidenefluoride (PVDF) membranes were purchased from Bio-Rad Laboratories Inc. (Hercules, CA, USA). Immobilon ECL Ultra Western HRP Substrate was purchased from EMD Millipore Corp. (Merck KGaA, Darmstadt, Germany). Primary antibodies for c-Myc (#5605), anti-Bcl-2 (#3498), cleaved-PARP (#5625), and β-actin (#4970), and HRP-conjugated anti-rabbit IgG (#7074) were purchased from Cell Signaling Technology (Beverly, MA). Milli-Q water (Millipore) was used in all stages of the study.

2.2. Synthesis of β-cyclodextrin-epichlorohydrin nanosponge (EpCN)

EpCN at molar ratio of 1 : 8 (β-CD: epichlorohydrin) was synthesized as described elsewhere[17] with slight modifications (Scheme 1). Briefly, β-CD (5 g) was dissolved in 33% (w/w) NaOH solution (8 mL) and stirred overnight at room temperature (RT). Then, the mixture was heated to 30 °C and immediately added epichlorohydrin (2.8 mL) under vigorous stirring. After stirring for 4 h, the reaction was stopped by the addition of acetone, which was subsequently removed by decantation. The reaction product was adjusted to pH 12 by the addition of 6 M HCl solution and kept at 50 °C overnight. After cooling, the pH of the reaction product was neutralised by the addition of 6 M HCl solution, followed by dialysis against deionized (DI) water using SnakeSkin™ Dialysis Tubing (10 K MWCO, 35 mm; Thermo Fisher Scientific) for 48 h at RT. After dialysis, the obtained EpCN solution was filtered using filter paper followed by lyophilized at −55 °C and 0.062 torr pressure (Alpha 1–2 LD plus, CHRIST, Germany) and kept in a desiccator at RT for future use.

2.3. Preparation of drug-loaded EpCNs

All formulations of drug-loaded EpCNs were prepared by loading the drug into EpCN at a constant weight ratio of 1 : 4 (drug : EpCN). First, the following solutions were prepared: 10 mg mL^{-1} of EpCN in Milli-Q water, 2 mg mL^{-1} of DX in Milli-Q water, and 25 mg mL^{-1} of EMD in absolute ethanol. After that, a total of 2 mg of DX or EMD was mixed with EpCN (8 mg) in Milli-Q water (2 mL) for the formulation of single

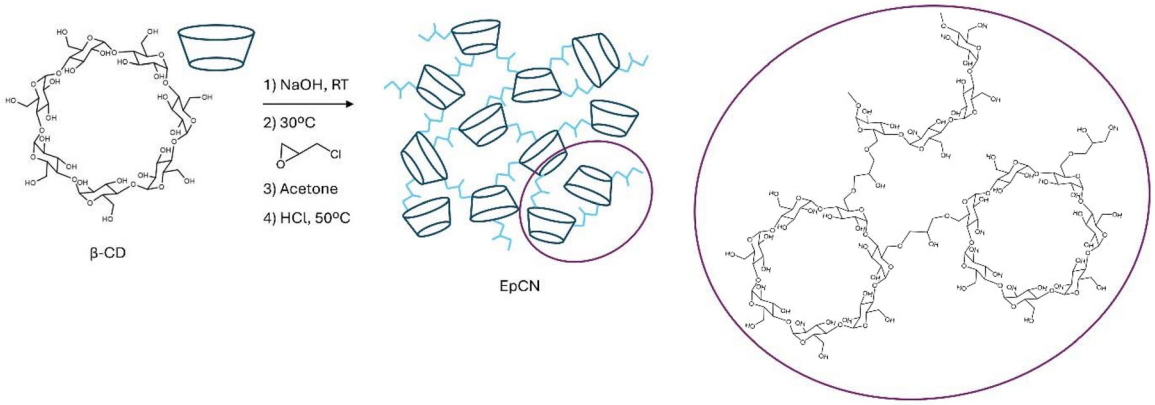

Scheme 1 Synthesis of β-cyclodextrin-epichlorohydrin nanosponge (EpCN).

drug-loaded EpCN, while DX (0.01 mg) and EMD (2.02 mg) were mixed with EpCN (8.12 mg) in Milli-Q water (2 mL) for dual drug-loaded EpCN (molar ratio of DX : EMD was 1 : 400). For the nanosponges containing EMD in the formulation (EMD-EpCN and DX/EMD-EpCN), 7 μL of 1 M HCl solution was added to enhance the dissolution of EMD in the mixture (final pH = 3.42). The mixture was stirred at 200 rpm for 24 h at RT in the dark. The resultant solution was subjected to filtration through a 0.45 μm polyethersulfone (PES) syringe filter to remove the insoluble fraction, then lyophilized (Alpha 1–2 LD plus), and stored in a desiccator at RT. The obtained drug-loaded EpCNs are denoted as DX-EpCN, EMD-EpCN, and DX/EMD-EpCN, corresponding to the drugs loaded into EpCN.

2.4. Encapsulation efficiency and drug loading capacity

The amount of DX and EMD loaded in EpCN was determined by UV-Vis spectrophotometry. A weighted amount (1 mg) of each drug-loaded EpCN was dissolved in 1 mL DMSO. The resulting solution was analysed using an UV-Vis spectrophotometer (JASCO V-730, JASCO International Co., Ltd, Japan) at 288 nm (EMD λ_{max}) and 480 mm (DX λ_{max}) after appropriate dilutions. The final concentration of each drug was calculated using a standard calibration curve (Fig. S1). The encapsulation efficiency (EE%) and drug loading capacity (LC%) were calculated with the following equations:

$$\%EE = \frac{\text{mass of drug loaded in EpCN}}{\text{mass of drug initial added}} \times 100$$

$$\%\ LC = \frac{\text{mass of drug encapsulated in EpCN}}{\text{mass of drug-loaded EpCN}} \times 100$$

2.5. Particle size (PS) polydispersibility index (PDI) and zeta potential (ZP)

The mean PS, PDI, and ZP of EpCN and drug-loaded EpCNs were determined with a Zetasizer Ultra (Malvern Panalytical Ltd, Malvern, UK). Data were processed using the Zetasizer Xplorer Software 3.3. All the sample was analyzed for three times to minimize errors.

2.6. Nuclear magnetic resonance (NMR) analysis

All samples were dissolved in D_2O and studied using 5 mm NMR tubes. All NMR data were collected on a Bruker AVANCE III NMR spectrometer (11.7 T) measured at 500 MHz frequency and equipped with a 5 mm $^1H/^{19}F$ BBI probe with actively shielded *z*-gradient that was used in combination with a Bruker gradient amplifier providing a maximum current of 10 A, which results in a 65 G cm^{-1} gradient. 1H diffusion NMR measurements (DOSY) were performed without sample spinning at 298 K, using stimulated echo with bipolar gradient pulses from Bruker's sequence library (ledbpgp2s) with the following parameters: 16k acquisition complex points, SW 14 ppm, NS 240, DS 16, D1 2 s, D20 (little delta) 0.6 s, P30 (big Delta/2) 1.8 ms, and 32 equally spaced gradient strengths from 5 to 95%.

2.7. Scanning electron microscopy (SEM)

SEM measurements were conducted on a JEOL SEM JSM-IT800HL (Tokyo, Japan) equipped with an energy dispersive X-ray spectroscopy (EDS) system, ULTIM EXTREME SEM, with AZTEC software from OXFORD INSTRUMENTS PLC & SUBSIDIARIES (Abingdon, UK). For SEM micrograph acquisitions, dilute solutions of samples (0.001 mg mL^{-1}) were prepared on Si wafer chips. Per each sample a 10 μL droplet was used. An accelerating voltage of 1.5 kV was used at a working distance of 5.3 mm. Secondary electron detector was used for all SEM micrograph acquisitions. Particle analysis is made possible by ImageJ (National Institutes of Health (NIH), Bethesda, MD, USA). For SEM/EDS acquisitions, freeze-dried samples were analyzed using an accelerating voltage of 5.00 kV at a working distance of 7.0 mm.

2.8. Atomic force microscopy (AFM)

AFM measurements were conducted by a Multimode 8HR (Bruker) equipped with fluid cell. Images were collected in Peak Force Tapping mode using Scanasyst Fluid + cantilever (Bruker). Samples were prepared on freshly cleaved mica modified by $MgCl_2$ incubating a solution of EpCN 0.1 mg ml^{-1} in

MQW for 30 min at RT and performing a washing by MQW to remove the excess of nanosponge in solution. Measurement parameters used during the experiments consist in Peak Force Frequency of 2 kHZ, Peak Force Setpoint between 250 pN–1 nN, scan rate of 0.5 Hz. Data were analysed by Nanoscope 2.0 software (Bruker).

2.9. *In Vitro* drug release study

The release of DX and EMD from dual drug-loaded nanosponge (DX/EMD-EpCN) under different pH conditions was evaluated by the dialysis method.[18] Briefly, DX/EMD-EpCN was dissolved in 100 mM phosphate buffer (PB) pH 5.8 and pH 7.4 at a concentration of 1 mg mL^{-1} of nanosponges (1.45 μM for DX and 0.62 mM for EMD). Two millilitres of DX/EMD-EpCN solution were added into a dialysis tube (Spectra-Por® Float-A-Lyzer® G2) and submerged in 13.5 mL of the corresponding buffer. The whole sample was kept at 37 °C and shaken at 200 rpm. All outer membrane buffer was collected (13.5 mL) and replaced with new pre-warmed buffer at various intervals (2 h, 5 h, 24 h, 48 h, 72 h, and 144 h) and then lyophilized (Alpha 1–2 LD plus). The lyophilized samples were reconstituted in 1 mL of Milli-Q water or DMSO to quantify the amount of DX and EMD, respectively. The concentration of released DX was determined by measuring the intrinsic fluorescence intensity using a spectrofluorometer (FS5, Edinburgh instruments) at emission wavelengths (λ_{em}) of 594 nm and excitation wavelengths (λ_{ex}) of 410 nm.[19] The concentration of released EMD was determined by UV-Vis spectrophotometry, as mentioned above. The amount of DX and EMD released was calculated from a calibration curve for DX (Fig. S2) and EMD (Fig. S1), respectively. Data were obtained as the average of two independent experiments. The cumulative drug release (%) was calculated with the following equation:

$$\text{Cumulative drug release (\%)} = \frac{\text{total amount of drug released (mg)}}{\text{initial amount of drug (mg)}} \times 100$$

2.10. Cell culture

The human lung cancer cells A549, human breast cancer MCF-7 cells and human lung fibroblast cells WI-38 were obtained from American Type Cell Culture (ATCC, Manassas, VA, USA). A549 and MCF-7 cells were cultured in Dulbecco's modified Eagle's medium (DMEM; Gibco, Waltham, MA, USA) and WI-38 cells were cultures in Eagle's Minimum Essential Medium (EMEM, Gibco). All culture media were supplement with 10% heat-inactivated fetal bovine serum (FBS, Gibco), GlutaMAX™ (Gibco), 1% penicillin/streptomycin solution (Gibco) and incubated in a humidified incubator at 37 °C with 5% CO_2. Cell media was replaced every 48 h and cells were split upon 80–90% confluence.

2.11. Cytotoxicity assay

Cancer cell lines A549 and MCF-7 cells were seeded at a density of 5×10^3 cells per well, and normal lung fibroblast cell lines WI-38 were seeded at 3×10^3 cells per well in 96-well plates and incubated for 24 h prior to treatment. To determine the half-maximal inhibitory concentration (IC_{50}) of free DX and EMD, A549 and MCF-7 cells were treated with (0–10 μM) 4-fold dilution concentrations of DX and (0–100 μM) 2-fold dilution concentrations of EMD for 72 h. To evaluate the cytotoxicity of drug-loaded EpCNs and their free drugs, cells were treated for 48 or 72 h with 0, 12.5, 25, 50, and 100 nM DX and 0, 5, 10, 20, and 40 μM EMD, either as free drugs (DX, EMD, or DX/EMD) or loaded in EpCNs (DX-EpCN, EMD-EpCN, and DX/EMD-EpCN). After treatment, cell viability was assessed using the SRB assay, as previously described.[20] The untreated cells served as a control group. Optical density (OD) was measured using a Synergy H1 multimode microplate reader (BioTek Instruments, Charlotte, NC, USA) at 540 nm with a reference wavelength of 690 nm. IC_{50} values were calculated by nonlinear regression analysis of dose–response curves using GraphPad Prism 8 (GraphPad Software, San Diego, CA, USA). The percentage of cell viability and cytotoxicity were calculated using the following equation:

$$\text{Cell viability (\%)} = \frac{\text{OD of treatment}}{\text{OD of control}} \times 100$$

$$\text{Cytotoxicity (\%)} = 100 - \text{cell viability (\%)}$$

2.12. Synergy determination

Drug combination studies were conducted using Chou's diagonal constant ratio scheme.[21] The optimal synergistic drug combination ratio was determined by using the equipotent molar ratio of DX : EMD in the combination analysis, as determined by the IC_{50} values obtained from individual treatments with DX and EMD in A549 cells. Cells were treated with concentrations corresponding to 0.125, 0.25, 0.5, 1, and 2 times the IC_{50} value of each individual drug and combination, across different constant ratios (1 : 1, 1 : 3, and 3 : 1), as shown in Table S1. Following 72 h of treatment, the cytotoxic effects of the drugs, both as single agents and in combination, were assessed by the SRB assay as described previously.[20] The Compusyn software (https://www.combosyn.com version 1.0) was utilized to generates the IC_{50}, dose reduction index (DRI) and combination index (CI) value for a particular combination of DX and EMD based on the cell viability data from the SRB assay, whereby additivity, synergy and antagonism were reflected by CI values of 1, <1, and >1, respectively.

2.13. Cell uptake study

Cell uptake studies were conducted using two cancer cell lines (A549 and MCF-7) and the normal lung fibroblast cell line (WI-38). Briefly, cells were seeded at a density of 2.5×10^5 cells per well in 6-well plates and incubated for 24 h, followed by treatment with either free DX/EMD or DX/EMD-EpCN at concentrations of 50 nM for DX and 20 μM for EMD. After 24 h of incubation, cells were washed with PBS and trypsinized. The trypsinized cells were then neutralized with complete medium (DMEM supplemented with 10% FBS), centrifuged at 300*g* for 5 min, and resuspended in 250 μL of PBS. Flow cytometry ana-

lysis was immediately performed using a MACSQuant10 flow cytometer (Miltenyi Biotec, Germany). The DX signal was measured using excitation with a 488 nm laser and detection with a 585 nm ± 40 nm filter. Data were analysed using Flowing Software (available at https://flowingsoftware.com/, Turku Bioscience, Finland).

2.14. Cell cycle analysis

A549 and MCF-7 cells were seeded in 6-well plates at a density of 2.5×10^5 cells per well and allowed to adhere for 24 h. A549 cells were then treated with drug-loaded EpCNs (DX-EpCN, EMD-EpCN, or DX/EMD-EpCN) at final concentrations of 125 nM for DX and 50 μM for EMD. MCF-7 cells were treated with 62.5 nM DX and 25 μM EMD. EMD and DX concentrations were selected for these studies taking into consideration the sensitivity of each cell line for the two drugs. After 48 h of treatment, cells were harvested by trypsinization, centrifuged at 300*g* for 5 min, fixed in cold 70% ethanol, and stored at −20 °C for at least 24 h. Before analysis, cells were centrifuged at 300*g* for 5 min and washed twice with PBS. Then, the cells were resuspended in a DAPI staining solution (0.1% Triton X-100 and 1 μg mL^{-1} DAPI in PBS) and incubated at RT in the dark for 30 min. Cell cycle distribution was analyzed using a MACSQuant10 flow cytometer (Miltenyi Biotec, Germany) and Flowing Software (Turku Bioscience, Finland).

2.15. Apoptosis analysis

A549 and MCF-7 cells were seeded in 6-well plates at a density of 2.5×10^5 cells per well and incubated for 24 h. Cells were then treated with drug-loaded EpCNs under the same conditions described for the cell cycle analysis. After 48 h of treatment, cells were collected and then stained with annexin V FITC (Thermo Fisher Scientific) and Zombie UV™ Fixable Viability Kit (BioLegend), following the manufacturer's instructions. Briefly, collected cells were incubated with fixable live/dead stain, Zombie UV (dilution 1 : 500 in PBS, BioLegend) at RT for 10 min in the dark. Next, cells were washed and incubated with annexin V FITC (Thermo Fisher Scientific) at RT for 15 min. Finally, washed cells were resuspended in 200 μL 1X Binding Buffer (Thermo Fisher Scientific) and fluorescence acquired on a MACSQuant10 flow cytometer (Miltenyi Biotec, Germany). Annexin V FITC was excited with the 488 nm laser and fluorescence collected at 525/50 nm. Zombie UV was excited by the 405 nm laser and fluorescence collected at 450/50 nm. The data were analyzed using Flowing Software (Turku Bioscience, Finland).

2.16. Western blot analysis

The expression levels of c-Myc, Bcl-2, and cleaved PARP were analyzed by western blotting, following a previously described protocol.[16] A549 and MCF-7 cells were seeded at a density of 2.5×10^5 cells per well in 6-well plates and incubated for 24 h. Cells were then treated with either drug-loaded EpCNs or unencapsulated drugs for 24 and 48 h. A549 cells were treated with 125 nM DX and 50 μM EMD, while MCF-7 cells were treated with 62.5 nM DX and 25 μM EMD. β-Actin served as the loading control. Protein bands were visualized using enhanced chemiluminescence (EMD Millipore Corp., Germany) and detected with the ChemiDoc™ MP Imaging System (Bio-Rad, USA). Band intensities were quantified using ImageJ software (NIH, Bethesda, MD, USA), and normalized values were expressed as fold change relative to untreated controls. Quantification was performed in two independent experiments.

2.17. Statistical analysis

The statistical computations and data compilation were conducted using GraphPad Prism software version 8.0 (GraphPad Software, Inc., La Jolla, CA, USA). The statistics were calculated using ordinary one-way or two-way ANOVA analysis. Dunnett's multiple comparisons test was utilised for the analysis of multiple comparisons. All experiments were performed in triplicate, with results expressed as mean ± standard deviation (SD). $P < 0.05$ was considered statistically significant.

3. Results and discussion

3.1. Synergistic cytotoxic effect of free DX and EMD in cancer cell lines

Prior to developing dual encapsulation DX and EMD, it is essential to evaluate whether the combination of the two drugs exhibits a synergistic effect. To establish effective combination therapies, the IC_{50} values for each drug were initially determined, as required by the Chou–Talalay method for drug combination analysis.[22] Cancer cell lines A549 and MCF-7 cells were exposed to increasing concentrations of DX and EMD, and viability was determined with the SRB assay. Dose–response curves indicate that DX (Fig. 1A) and EMD (Fig. 1B) suppressed cell viability in a dose-dependent manner in both cell lines. The IC_{50} values generated from these graphs are presented in Fig. 1C. The IC_{50} of DX and EMD on A549 was found to be 105 nM and 38.27 μM, respectively, while on MCF-7 cells it was found to be 76 nM and 24.97 μM, respectively. Based on IC_{50} data on A549 and MCF-7 cells, both cell lines showed a comparable response to DX, whereas A549 cells appeared to be less sensitive to EMD than MCF-7 cells. Therefore, we conducted further studies on the synergistic cytotoxic effect of the DX and EMD combination, focusing on A549 cells.

We further investigated the effect of the DX and EMD combination to verify their anti-cancer activity and synergism toward A549 cells as well as determined optimal synergistic drug combination ratio. The cells were treated with DX and EMD at various equipotent molar ratios derived from their respective IC_{50} values (DX: EMD (IC_{50})) in order to determine the optimal synergistic drug combination ratio. Three difference combination ratios were selected: 1 : 1, 1 : 3, and 3 : 1, corresponding to the following concentrations: 100 nM/40 μM, 100 nM/120 μM, and 300 nM/40 μM (DX/EMD), respectively. A549 cells were treated according to these ratios with increasing concentrations of both drugs separately and combined, and cell viability was determined using the SRB assay at 72 h.

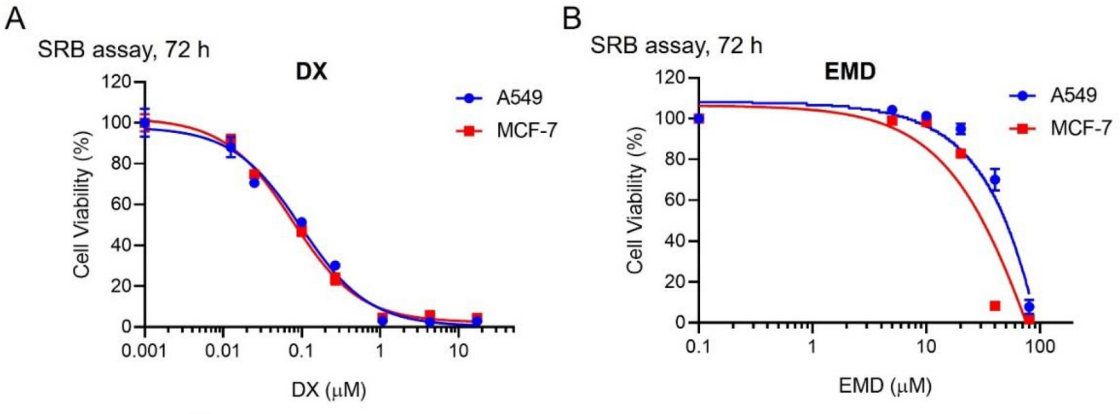

C

Cell line	IC_{50} (μM) ± SD	
	DX	EMD
A549	0.105 ± 0.013	38.27 ± 4.70
MCF-7	0.076 ± 0.005	24.97 ± 3.61

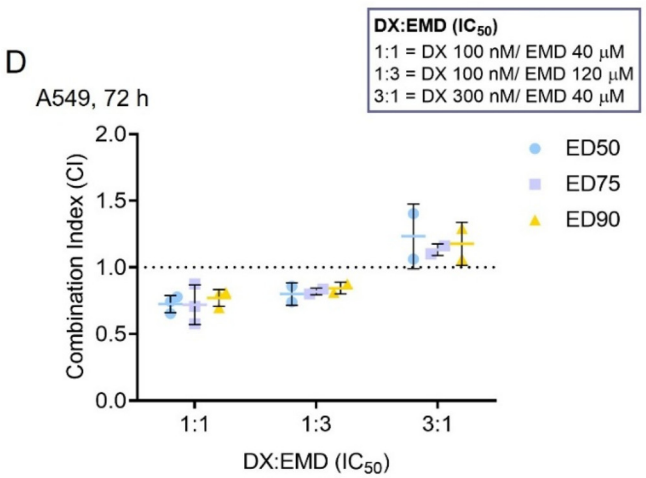

Fig. 1 Cytotoxicity of free DX and EMD on cancer cell lines A549 and MCF-7. The dose-respond curves of free DX (A) and EMD (B) towards A549 and MCF-7 cells, at different concentrations for 72 h. Cell viability was determined by SRB assay. (C) Table representation IC_{50} for A549 and MCF-7 cells. (D) Combination index (CI) values for different combination ratios derived from IC_{50} values (DX : EMD (IC_{50})) at ED50, ED75, and ED90 were calculated using CompuSyn software.

The combination index (CI) at 50%, 75%, and 90% effective doses (ED) was then calculated using the CompuSyn software.[21] As shown in Fig. 1D, the combination of DX and EMD at ratios of 1 : 1 and 1 : 3 demonstrated synergistic cytotoxicity effect on A549 cells (CI < 1) across all effective doses. In contrast, the 3 : 1 ratio did not exhibit synergistic effect, indicating a potential loss of efficacy with higher DX proportions. Among the synergistic combinations, the 1 : 1 ratio has shown a higher synergism (CI ~0.7) compared to the 1 : 3 ratio (CI ~0.8) (Table S1). These results suggest that the synergistic effect diminishes with increasing DX content, highlighting the importance of optimizing drug ratios for combination therapy. Based on these findings, the 1 : 1 ratio, corresponding to 100 nM DX and 40 μM EMD (1 : 400 molar ratio), was selected for the formulation of the dual drug-loaded cyclodextrin nanosponge.

3.2. Physicochemical characterization of drug-loaded EpCNs

To obtain single and dual drug-loaded nanosponges, β-cyclodextrin (βCD)-epichlorohydrin (EP) nanosponges (EpCN) were first prepared by crosslinking βCD with EP. Then, DX, EMD, or DX/EMD combination was loaded to EpCN (1 : 4 weight ratio); the obtained EpCN formulations were named DX-EpCN, EMD-EpCN, and DX/EMD-EpCN, respectively.

DLS measurements showed average *Z*-values for EpCNs with and without loaded drugs of approximately 10 nm, with a

high polydispersity (PDI > 0.5) (Table S2). A more detailed analysis of the intensity and number distributions revealed scattering peaks at around 10 nm and 250 nm in the intensity distribution (Fig. 2A (left)). However, the 250 nm peak disappeared completely in the number distribution, confirming that the actual size of the nanosponges is approximately 10 nm. The number distribution for EpCNs is shown in Fig. 2A (right). Atomic Force Microscopy (AFM) imaging, performed in liquid mode on EpCNs deposited on mica, revealed particle diameters between 10 and 30 nm and heights of approximately 2 nm (Fig. 2B and Table S3). Additionally, SEM particle analysis (Fig. 2C) of EpCN with and without drugs demonstrated average particle size of around 30, respectively (Table S4). A slight mismatch in sizes between the AFM and DLS measurements was observed, likely due to image drift during AFM scanning, and some spreading of the EpCNs on

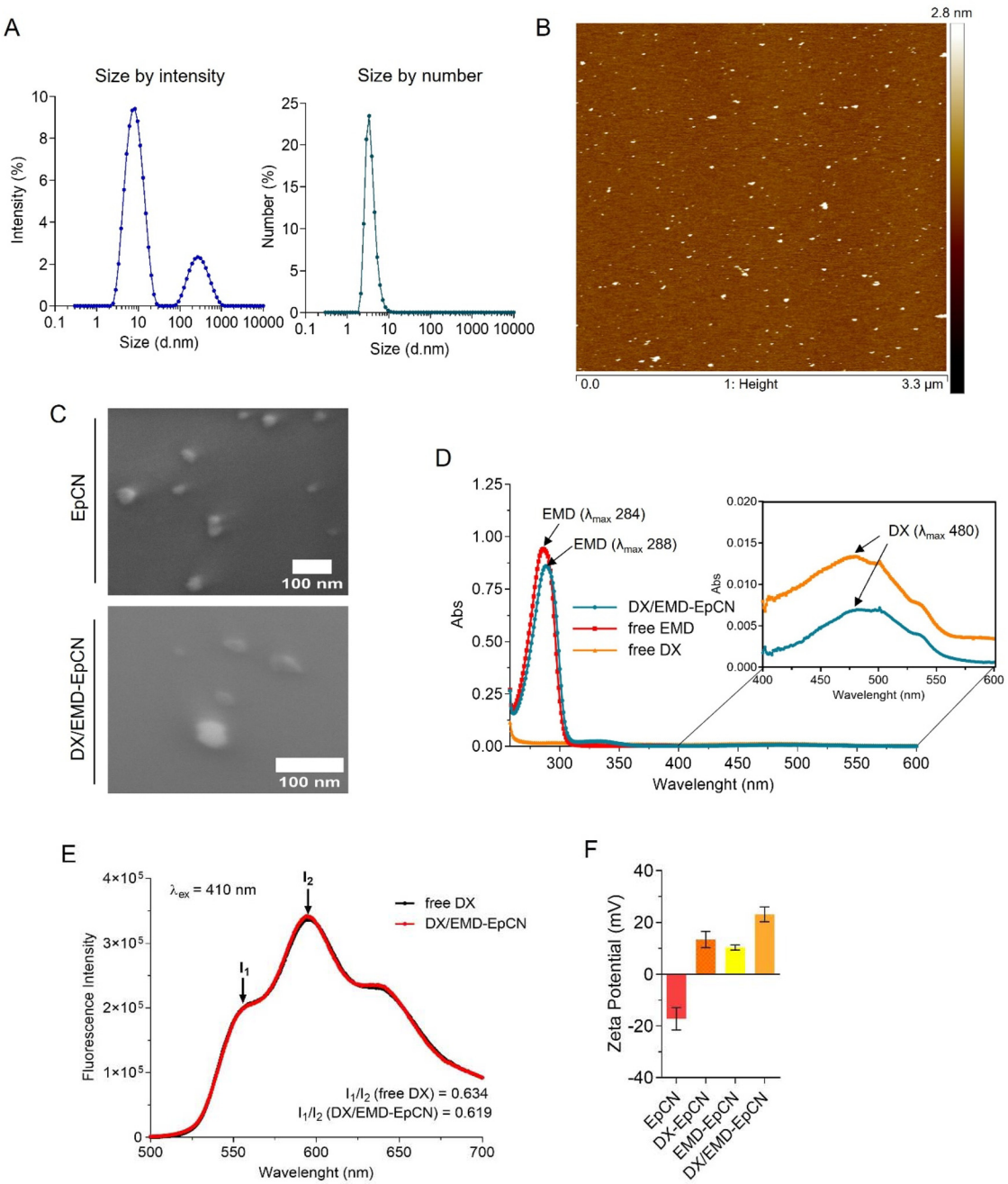

Fig. 2 Physicochemical characterization of drug-loaded EpCNs. (A) Size distribution histograms by size (left) and number (right) of blank nanosponge obtained from DLS. (B) AFM image of EpCN. (C) SEM images of EpCN and DX/EMD-EpCN. (D) UV-Vis spectra of free EMD, free DX, and DX/EMD-EpCN in DMSO. Inset: zoom image of DX peak at 480 nm of free DX and DX/EMD-EpCN. (E) Fluorescence spectra of free DX and DX/EMD-EpCN in water, where $I_1 = \lambda_{em}$ 560 nm and $I_2 = \lambda_{em}$ 590 nm. (F) Zeta potential of EpCN and three formulations of drug-loaded EpCNs.

the surface of the mica. Similarly for SEM the EpCNs may spread on the holder after vacuum resulting in a slightly larger size. Some aggregation during drying can also not be ruled out. However, all techniques consistently demonstrate that the EpCN and DX/EMD-EpCN have sizes below 50 nm.

DLS of EpCN and drug-loaded EpCN (DX/EMD-EpCN) in cell culture media containing serum (DMEM + 10% FBS) was also performed (Fig. S3). The media itself exhibited strong scattering from proteins and protein aggregates. Upon addition of EpCNs to protein-containing media, the DLS intensity and number distributions were indistinguishable from those of the media alone, suggesting that the scattering of EpCNs was completely masked by protein scattering. Importantly, we did not observe any additional peaks that would indicate large-scale aggregation, although such signals could also be masked by protein scattering. Instead, for DX/EMD-EpCN, we observed changes in scattering patterns compared to media alone, which were also dependent on nanosponge concentration. Scattering intensity shifted to higher values as the concentration of loaded nanosponges increased, with a single peak centered around 100 nm at 1.5 mg mL^{-1}. The number distribution also shifted with increasing concentration but remained below 100 nm (approximately 36 nm), consistent with the formation of small aggregates of loaded EpCNs. The reason for this difference in behaviour we believe comes from EMD and DX loading that brings positive charges, which can promote protein binding and also lead to aggregation as concentration of EpCNs increases (Fig. S3). These results suggest that EpCNs may interact with cells predominantly in the form of small aggregates, but still within the nanometre size range.

SEM/EDS analysis at individual EPCNs (Fig. S4) confirmed the incorporation of carbon-based nitrogen-containing species into the EpCN as the carbon-to-oxygen atomic ratio, C/O, increases from 2.20 (EpCN) to 2.74 (DX/EMD-EpCN). The detection of nitrogen (0.64 at%) present in DX/EMD-EpCN, proves the drug encapsulation as N is only present in EMD and DX but not in the nanosponges.

UV-Vis spectroscopy was employed to confirm the presence of both DX and EMD in the DX/EMD-EpCN formulation. Following dissolved DX/EMD-EpCN in DMSO, the absorption peak of EMD exhibited a slight red shift from 284 nm to 288 nm, indicating possible interactions with the solvent or the nanosponge matrix. In contrast, no significant shift was observed in the absorption peak of DX (Fig. 2D). We also compared fluorescence spectra of DX/EMD-EpCN with free DX. The typical fluorescence spectra of DX are displayed with peaks at 560 (I_1) and 590 nm (I_2), with the most prominent peak at 590 nm (Fig. 2E). The ratio of these peaks (I_1/I_2) is sensitive to the polarity of the environment.[19] Since the I_1/I_2 ratio for free and encapsulated DX are the same, we can conclude that DX is trapped at hydrophilic cavities or between β-CD of the nanosponge. A sketch of the EpCN with DX encapsulated in hydrophilic sites and EMD in hydrophobic pockets is shown in Scheme 2.

The zeta potential measurements indicated that the surface charge of the blank nanosponge was negative and became positive after drug loading. In particular, the dual drug-loaded

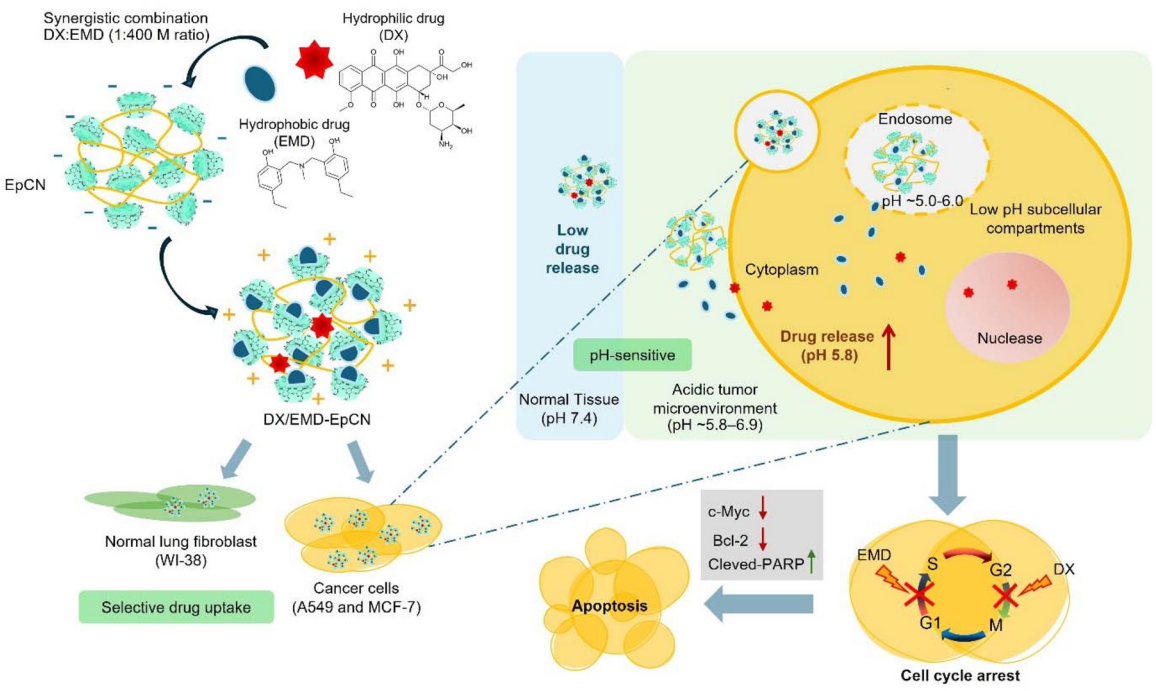

Scheme 2 Scheme of nanosponge formulation with EMD and DX, and experimental approach followed biological studies, summarizing main results.

formulation (DX/EMD-EpCN) exhibited a greater positive charge compared to the single drug-loaded EpCNs (DX-EpCN and EMD-EpCN) (Fig. 2F). The reversal of the charge is due to the loaded drugs that are positively charged in the conditions of the loading.

We further confirmed the structure of DX/EMD-EpCN and the interaction between drugs with the nanosponge using ^{1}HNMR, DOSY and NOESY analysis. First, ^{1}HNMR experiments were carried out on epichlorohydrin, β-CD and EpCN. Comparison of the three NMR spectra did not show the presence of no-reacted epichlorohydrin and β-CD in EpCN purified samples (Fig. S5). Broad EpCN signals (3.25–4.25 ppm and 4.75–5.25 ppm) suggest the formation of a crosslinked macromolecule. No broad epichlorohydrin signals were detected in the EpCN spectra in the range of 2.7–3 ppm because, after nucleophilic addition of the negative charged β-CD hydroxyl group, epichlorohydrin turned into a glycerol derivative whose NMR bands overlap with β-CD in 3.5–3.8 ppm. ^{1}HNMR was carried out to study encapsulation of doxorubicin into hydrophobic β-CD pockets of EpCN (Fig. S6). DX signals in DX-EpCN undergo chemical shifts in both aromatic (7.5–7.8 ppm) and aliphatic (1–3 ppm) DX regions. To study in more detail DX encapsulation into EpCN, DOSY and NOESY experiments on DX-EpCN were also performed. Fig. S7 show overlapping of three independent DOSY experiments (DX, green; EpCN, purple; DX-EpCN, red). Diffusion depends on MW, so as expected, DX alone diffuse faster (D = 1.99 × 10^{-6}) than EpCN and DX-EpCN (D = 8.98 × 10^{-7}) and, most important, no free DX was detected in the DX-EpCN sample. NOESY experiment of DX-EpCN (Fig. S8) do not show any cross peaks between DX and cyclodextrin excluding no close interaction (less than 5 Å) between DX and EpCN. Taking together NMR and fluorescence data, we can conclude that DX is encapsulated in EpCN hydrophilic regions and not in the hydrophobic β-CD pockets. A NOESY experiment with EMD-EpCN was also carried out (Fig. S9), The presence of cross peaks between EMD and cyclodextrin protons suggest encapsulation of EMD into hydrophobic cyclodextrin pockets. Once confirmed that DX is encapsulated in hydrophilic regions of DX-EpCN and EMD encapsulated into hydrophobic pockets of EpCN, we moved to study EpCN encapsulated with both drugs (DX/EMD-EpCN). NOESY of DX/EMD-EpCN (Fig. 3) indicate the presence of both drugs, cross-peaks with Ep-CN confirm that EMD is encapsulated into EpCN hydrophobic pockets while absence of cross-peaks with Ep-CN prove the encapsulation of DX into hydrophilic regions of EpCN.

3.3. *In vitro* drug release profile of DX/EMD-EpCN

The main purpose of nanocarrier development is the controlled release and delivery of therapeutic drugs to targeted sites with reduced systemic toxicity. Profiting from the pH difference between normal tissue (pH 7.4) and the more acidic tumour microenvironment (pH 5.8–6.9) for triggering drug

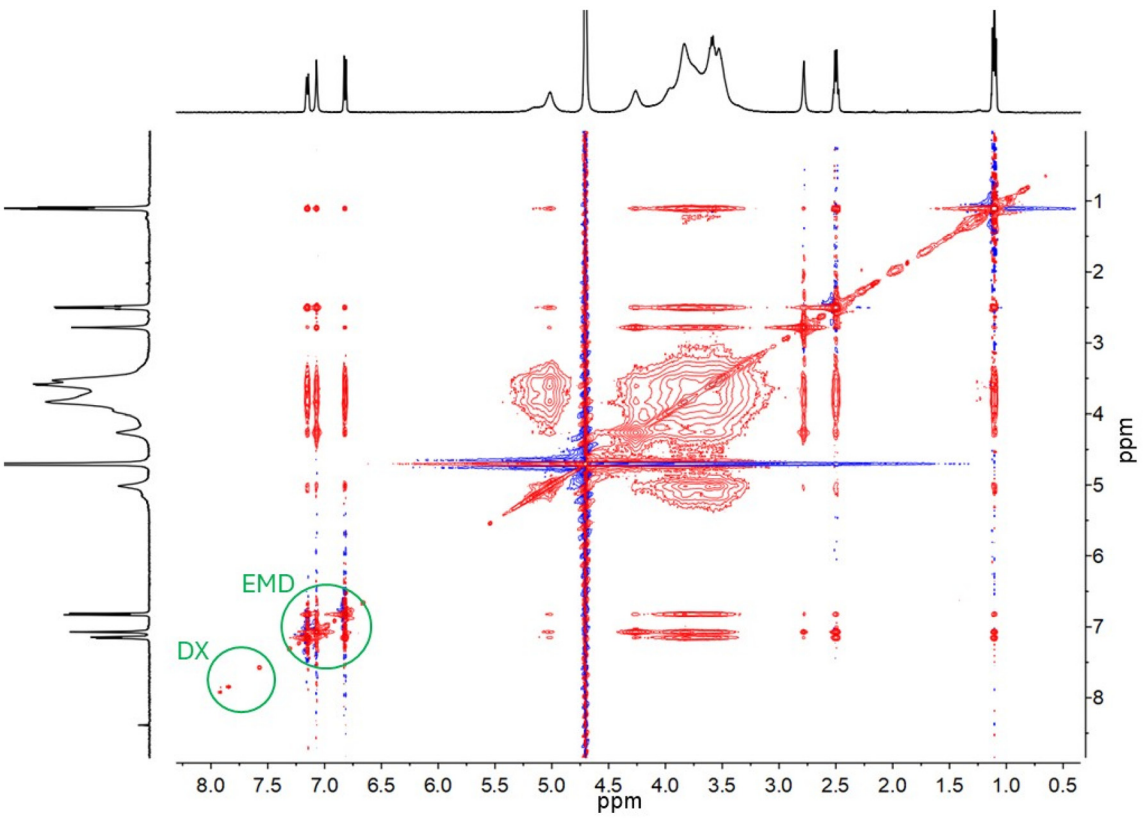

Fig. 3 NOESY NMR experiment of DX/EMD-EpCN (D_2O).

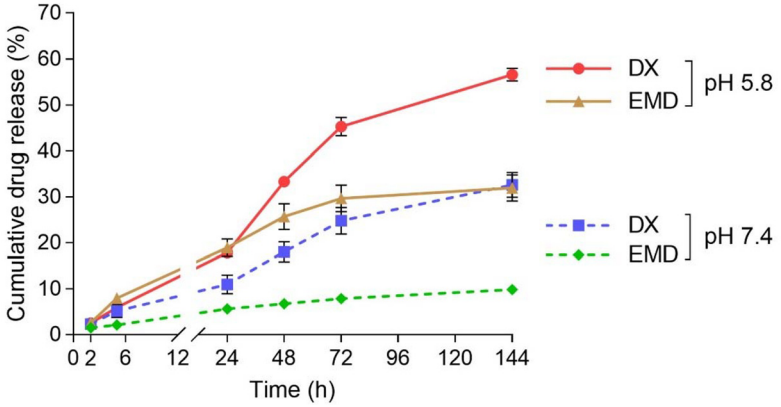

Fig. 4 *In vitro* release profile of DX and EMD from DX/EMD-EpCN in 100 mM phosphate buffer at pH 5.8 and pH 7.4 (n = 2).

delivery is one effective approach for selective delivery into tumors.[23,24] Furthermore, pH lowering in subcellular compartments such as endosomes and lysosomes results in even lower pH values (5.0–6.0), which serve as internal stimuli for the pH-triggered release from nanocarrier systems.[25,26] To investigate the pH sensitivity of DX/EMD-EpCN, a release study was conducted at 37 °C under different pH conditions (pH 5.8 and pH 7.4) for 5 days. These pH conditions are consistent with physiological conditions (pH 7.4) and tumour microenvironment (5.8).[27] As shown in Fig. 4, the *in vitro* release of DX and EMD from DX/EMD-EpCN at pH 5.8 was higher compared to pH 7.4. At pH 5.8, DX and EMD were released to a 45% and 30%, respectively, at 72 h. Whereas, at pH 7.4, DX and EMD were released only at a 25% and an 8%, respectively. Thus, DX/EMD-EpCN indicates pH-sensitive release of DX and EMD from the nanosponge that may diminish systemic side effects of chemotherapeutic drugs. Moreover, when comparing the *in vitro* release profiles of DX and EMD from DX/EMD-EpCN, DX was released from the nanosponge faster than EMD under all pH conditions. This could be attributed to the different encapsulation sites of the two compounds in the nanosponge. DX is encapsulated within hydrophilic regions, which facilitated its diffusion and release, whereas EMD is confined within hydrophobic cavities of β-CD in the nanosponge, which results in a slower release profile. Although DX and EMD have different release rates, both drugs were sustained released at a synergistic concentration ratio of DX and EMD (1 : 400–1 : 1200 molar ratio), therefore preserving a synergistic combination over the release period. Thus, the sustained and gradual release behaviour of DX/EMD-EpCN supports prolonged therapeutic activity, potentially enhancing the overall efficacy of the drug formulation.

3.4. Enhanced cytotoxicity and synergistic efficacy of DX/EMD-EpCN in cancer cell lines

Next, the cytotoxic effects of drug-loaded EpCNs were evaluated and compared to their free drugs in the cancer cell lines A549 and MCF-7. The SRB assay was used to investigate cytotoxicity. The cells were exposed to different concentrations of free drugs (DX, EMD, and DX/EMD) and drug-loaded EpCNs (DX-EpCN, EMD-EpCN, and DX/EMD-EpCN) for 72 h. We found that blank EpCN did not induce cytotoxicity (cell viability > 80%) against both A549 and MCF-7 cells until doses of 2 mg mL^{-1} (Fig. S10). As the highest dose of drug-loaded EpCNs used in this study contained EpCN less than 0.25 mg mL^{-1}, it can be concluded that EpCN alone does not affect cell viability, indicating that the drug delivery system is safe. As shown in Fig. 5A and B, all treatments with drug-loaded EpCN resulted in a significant dose-dependent reduction of cell viability in both A549 and MCF-7 cells after 72 h. In A549 cells, at 50 nM DX and 20 μM EMD, DX/EMD-EpCN treatment led to cell viability of 22.8%, whereas DX/EMD, DX-EpCN, and EMD-EpCN treatments showed cell viability of 50.4%, 50.3%, and 61.1%, respectively (Fig. 5A). Similarly, in MCF-7 cells under the same treatment conditions, DX/EMD-EpCN significantly reduced cell viability to 11.3%, while DX/EMD, DX-EpCN, and EMD-EpCN treatments resulted in cell viability of 59.4%, 63.8%, and 14.8%, respectively. These results indicate that co-encapsulation of DX and EMD in EpCN has a considerable synergistic effect in reducing cell viability, particularly in MCF-7 cells.

We also investigated the improved therapeutic potential of DX alone, EMD alone, and combination after encapsulated in EpCN. Based on the SRB results, the IC_{50} value, dose reduction index (DRI), and CI values were calculated using Compusyn software[21] and are summarized in Table 1. For single-drug treatments, the IC_{50} of DX decreased from 0.15 μM to 0.06 μM in A549 cells, and from 0.12 μM to 0.06 μM in MCF-7 cells after single encapsulation. Likewise, EMD demonstrated a significant reduction in IC_{50} following encapsulation, from 43.84 μM to 22.81 μM in A549 cells and from 20.62 μM to 13.14 μM in MCF-7 cells. Treating cells with a combination of free Dox and EMD resulted in significant increased cytotoxicity in both A549 and MCF-7 cells, and it caused a more pronounced cytotoxicity when encapsulated in EpCN. In combination treatment, the IC_{50} of DX was reduced from 0.04 μM to 0.02 μM in A549 and MCF-7 cells after co-encapsulation. Also, dual encapsulation of DX and EMD decreased the IC_{50} of EMD

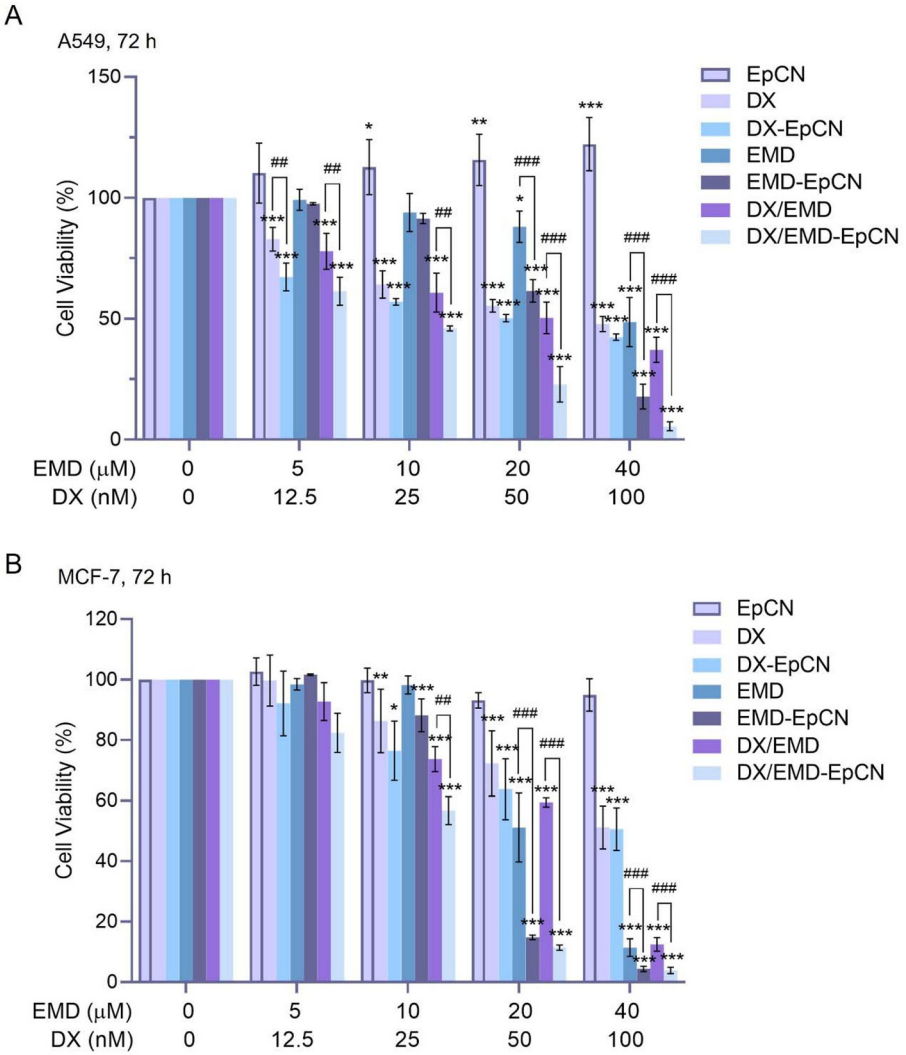

Fig. 5 Cytotoxicity of free drugs and drug-loaded EpCN formulations against A549 and MCF-7 cells. Cell viability of A549 (A) and MCF-7 cells (B) after treatment with EpCN (empty nanosponge), drug-loaded EpCNs and their free-form for 72 h. Cell viability in was assessed using the SRB assay. $^{*}p < 0.05$, $^{**}p < 0.01$, $^{***}p < 0.001$ compared to the untreated control group; $^{\#\#}p < 0.01$, $^{\#\#\#}p < 0.001$ compared to drug-loaded EpCN groups.

Table 1 Results of IC_{50}, DRI, and CI values for drug combination by DX and EMD, as free drugs or encapsulated in nanosponge (EpCN) in A549 and MCF-7 cell lines

		A549		MCF-7	
Drug		Free drug	Drug-EpCN	Free drug	Drug-EpCN
IC_{50} (μM) Single drug	DX	0.15 ± 0.05	0.06 ± 0.01*	0.12 ± 0.01	0.06 ± 0.00**
	EMD	43.84 ± 1.25	22.81 ± 3.31***	20.62 ± 2.14	13.14 ± 1.29**
IC_{50} (μM) combination	DX	0.04 ± 0.01	0.02 ± 0.01*	0.04 ± 0.005	0.02 ± 0.01*
	EMD	17.77 ± 4.23	9.05 ± 2.39*	14.66 ± 2.05	6.29 ± 3.62*
DRI[a] combination	DX	3.32 ± 0.61	6.50 ± 0.97**	3.34 ± 0.88	8.21 ± 1.42**
	EMD	2.55 ± 0.68	5.04 ± 1.40*	1.45 ± 0.62	3.12 ± 0.82*
CI value[b]		0.71 ± 0.05	0.36 ± 0.04***	1.07 ± 0.24	0.58 ± 0.14*

$^{*}p < 0.05$, $^{**}p < 0.01$, and $^{***}p < 0.001$; free drug *vs.* drug-loaded EpCNs. [a] Dose reduction index (DRI) was calculated from the DRI equation and algorithm using CompuSyn software. DRI = 1, >1, and <1 indicates no dose-reduction, favorable dose-reduction, and not favorable dose-reduction, respectively, for each drug in the combination. [b] Combination index (CI) was calculated from the CI equation algorithms using CompuSyn software. CI = 1, <1 and >1 indicates additive effect, synergism and antagonism, respectively.

from 17.77 μM to 9.05 μM in A549 and from 14.66 μM to 6.29 μM in MCF-7 cells (Table 1). The DRI values demonstrated that the dual encapsulation of DX and EMD in EpCN enables substantial dose reductions in combination therapy. In A549 cells, the DRI for DX increased from 3.32 (free drug) to 6.50 (encapsulation), and the DRI for EMD increased from 2.55 to 5.04. Similarly, for MCF-7 cells the DRI for DX rised from 3.34 to 8.21, and the DRI for EMD increased from 1.45 to 3.12. The CI values confirmed the synergistic potential of the dual drug-loaded EpCN formulation. In A549 cells, CI value decreased from 0.71 (free drug combination) to 0.36 following co-encapsulation, demonstrating a significant synergistic interaction (CI < 1). In MCF-7 cells, encapsulation enhanced CI value from 1.07 (slight antagonism) to 0.58 (synergism), demonstrating a significant shift towards synergism. The results indicate that EpCN encapsulation significantly increases the cytotoxic efficacy of both DX and EMD, especially in combination therapy (dual encapsulation).

Taken together, drug encapsulation in nanosponge, as a single or combination treatment of DX and EMD, reduces the effective drug concentration needed (lower IC_{50}), enhances dose efficiency (higher DRI), and facilitates synergistic interactions (lower CI values) in cancer cell lines. Thus, it highlights the effectiveness of EpCN as a delivery system for combination chemotherapy strategies.

3.5. Drug-loaded EpCNs selectively increases cytotoxicity and cellular uptake in cancer cells

Having observed that loading DX and EMD as a single or dual encapsulation into EpCN can enhance their therapeutic potential in both cancer cell lines A549 and MCF-7, we further investigated whether drug-loaded EpCNs have selective targeted cytotoxicity against cancer cells compared to normal cells, as sketched in Scheme 2. The selective cytotoxic activity of drug-loaded EPCN formulations was evaluated using the two cancer cell lines (A549 and MCF-7) and normal lung fibroblast cell lines (WI-38). The cells were treated with either free drugs (DX, EMD, and DX/EMD) or drug-loaded EpCNs (DX-EpCN, EMD-EpCN, and DX/EMD-EpCN) for 48 and 72 h. The SRB assay was used to assess cell viability. Fig. 6A and C demonstrate that all drug-loaded EpCNs treatments resulted in a significant decrease cell viability in time-dependent manner in both A549 and MCF-7 cells when compared to their free drugs. After 48 h of treatment, the dual drug-loaded nanosponge

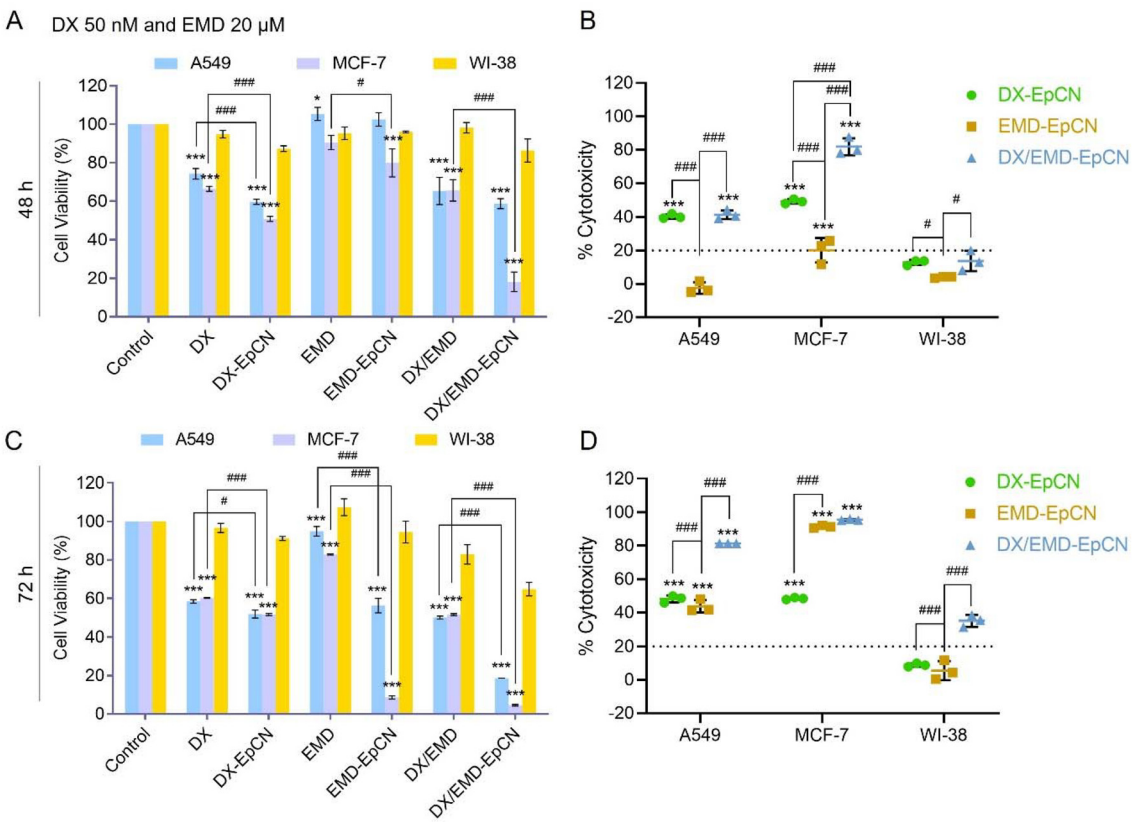

Fig. 6 Comparative cytotoxicity of free drugs and drug-loaded EpCN formulations in cancer and normal cell lines. Cell viability and cytotoxicity were assessed in A549 (lung cancer), MCF-7 (breast cancer), and WI-38 (normal lung fibroblast) cell lines following treatment with DX, EMD, their combination (DX/EMD), and EpCN-encapsulated formulations (DX-EpCN, EMD-EpCN, DX/EMD-EpCN) for 48 and 72 h. (A and C) Cell viability percentages were determined using the SRB assay at 48 h (A) and 72 h (C). (B and D) Cytotoxicity was expressed as percentage non-viable cells (100% – viability) at 48 h (B) and 72 h (D). *$p < 0.05$, **$p < 0.01$, ***$p < 0.001$ compared to the untreated control group (A and C) or control normal cells WI-38 (B and D); $^{\#}p < 0.05$, $^{\#\#}p < 0.01$, $^{\#\#\#}p < 0.001$ compared between groups as indicated.

(DX/EMD-EpCN) showed significant cytotoxicity, and cell viability decreased to below 60% in A549 and to below 30% in MCF-7 cells (Fig. 6A) and further reducing to below 20% in both cancer cell lines (Fig. 6C). In contrast, free drug treatments (DX, EMD, and DX/EMD) resulted in only moderate cytotoxicity, showing cell viability above 40% in both A549 and MCF-7 cells after 72 h. When compare between each drug-loaded EpCN formulations, DX/EMD-EpCN most significantly enhanced cytotoxic effects in cancer cells while preserving normal cells at both time point (Fig. 6B and D). As shown in Fig. 6D, DX/EMD-EpCN resulted in cytotoxicity above 75% in both A549 and MCF-7 cells at 72 h, whereas cytotoxicity in WI-38 cells remained below 30% (Fig. 6D). Additionally, single-drug encapsulated nanosponge (DX-EpCN and EMD-EpCN) exhibited enhanced cytotoxicity in cancer cells, with negligible effects on WI-38 cells. Thus, EpCN enhances the therapeutic specificity of chemotherapeutic drugs (DX and EMD) by targeting cancer cells and minimising off-target toxicity in normal cells.

The enhanced cytotoxicity of DX/EMD-EpCN could be associated with various potential mechanisms. Nanocarriers, including cyclodextrin-based nanosponges, enhance drug delivery through the promotion of endocytosis-mediated internalization, resulting in elevated drug concentrations inside the cells.[28,29] Cancer cells demonstrate elevated metabolic activity and augmented endocytic pathways, resulting in an increased internalisation of nanoparticles compared to normal cells.[30] We next evaluate whether the EpCN enhanced drugs internalization with selectivity towards cancer cells. The cellular uptake of DX by A549, MCF-7, and WI-38 cells was quantified using flow cytometry after 24 h of treatment with either free drugs (DX/EMD) or the EpCN formulation (DX/EMD-EpCN) at concentrations of 50 nM DX and 20 μM EMD (Fig. 7A and B). In A549 cells, the percentage of DX-positive cells increased from approximately 7.7% with free DX/EMD to 12.8% following EpCN encapsulation. In MCF-7 cells, the percentage of DX-positive cells also significantly increased from 9.8% to 20.5% with the nanosponge formulation (Fig. 7B). The results indicate that EpCN increased to about the double the intracellular accumulation of DX in both cancer cell types. On the other hand, the uptake in normal WI-38 fibroblast cells was significantly lower. While free DX/EMD treatment resulted in 2.7% DX-positive cells, the EpCN formulation slightly increased to 3.2% of DX-positive cells (Fig. 7B). This limited uptake in normal cells demonstrates that the enhanced delivery effect of EpCN is more pronounced in cancer cells, suggesting selective targeting. The findings indicate that EpCN encapsulation improves the cellular uptake of DX specifically

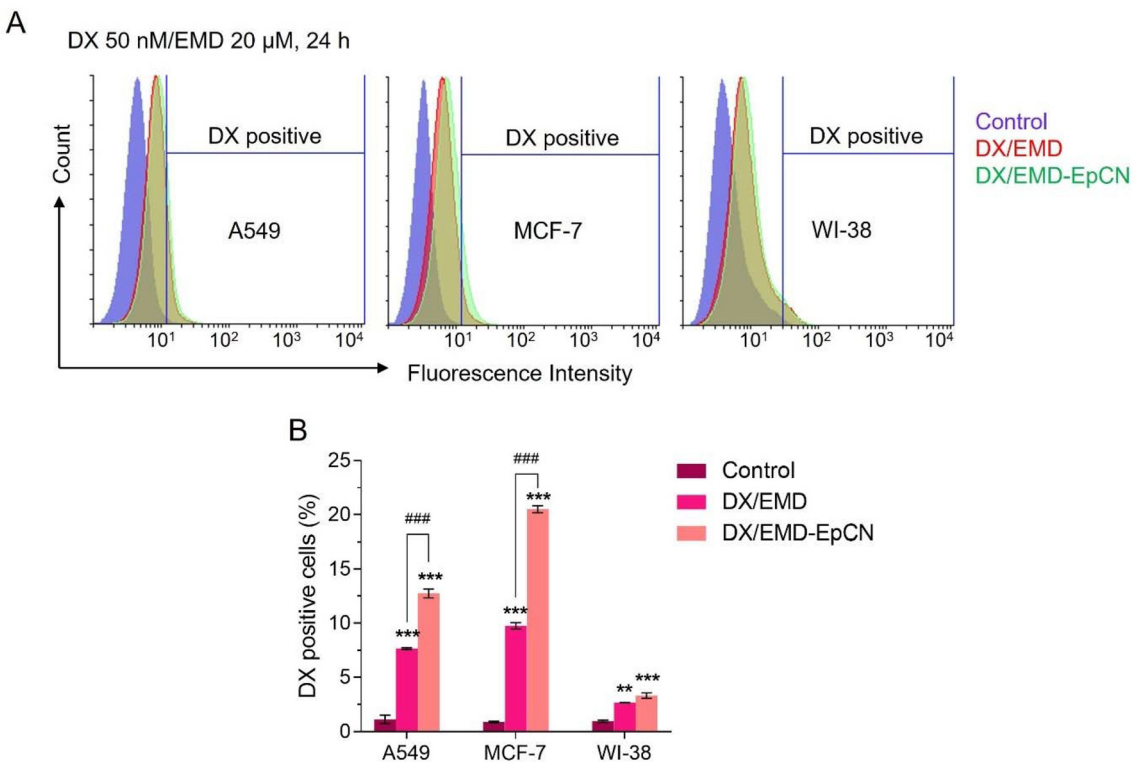

Fig. 7 Cellular uptake of doxorubicin (DX) in A549, MCF-7, and WI-38 cells after treatment with dual drug-loaded nanosponge (DX/EMD-EpCN) and their free drugs (DX/EMD). Flow cytometry was used to quantify the uptake of free DX or DX/EMD-EpCN by cells. (A) overlay histograms represent the fluorescence intensity of DX in each cell type as indicated after treated with DX/EMD or DX/EMD-EpCN at concentrations of 50 nM DX and 20 μM EMD for 24 h. A rightward shift indicates increased intracellular accumulation of DX. (B) Quantitative analysis of DX-positive cells (%) from A. Data are presented as mean ± SD. $^{**}p < 0.01$, $^{***}p < 0.001$ compared to the untreated control group; $^{\#\#\#}p < 0.001$ compared between groups as indicated.

in cancer cells, likely attributable to an increase endocytic activity and mechanisms associated with tumour uptake. Taken together, EpCN enhanced the cellular uptake of DX compared to free DX in both cancer cell lines A549 and MCF-7, which might explain the strong cytotoxicity effect seen in earlier experiment, as well as the selective uptake by cancer cells over normal cells. Thus, EpCN could be an effective tumor-targeted delivery system for chemotherapeutic drugs DX and EMD.

3.6. Dual drug-loaded EpCN induces superior cell cycle arrest and apoptosis compared to single drug-loaded EpCNs

Given enhanced DX/EMD-EpCN cytotoxicity and synergistic effects, the molecular mechanisms underlying these results require further investigation. Chemotherapeutic agents primarily exert their anticancer effects by disrupting the cell cycle, resulting in growth arrest and apoptosis.[31] To investigate whether DX/EMD-EpCN is associated with modulation of cell

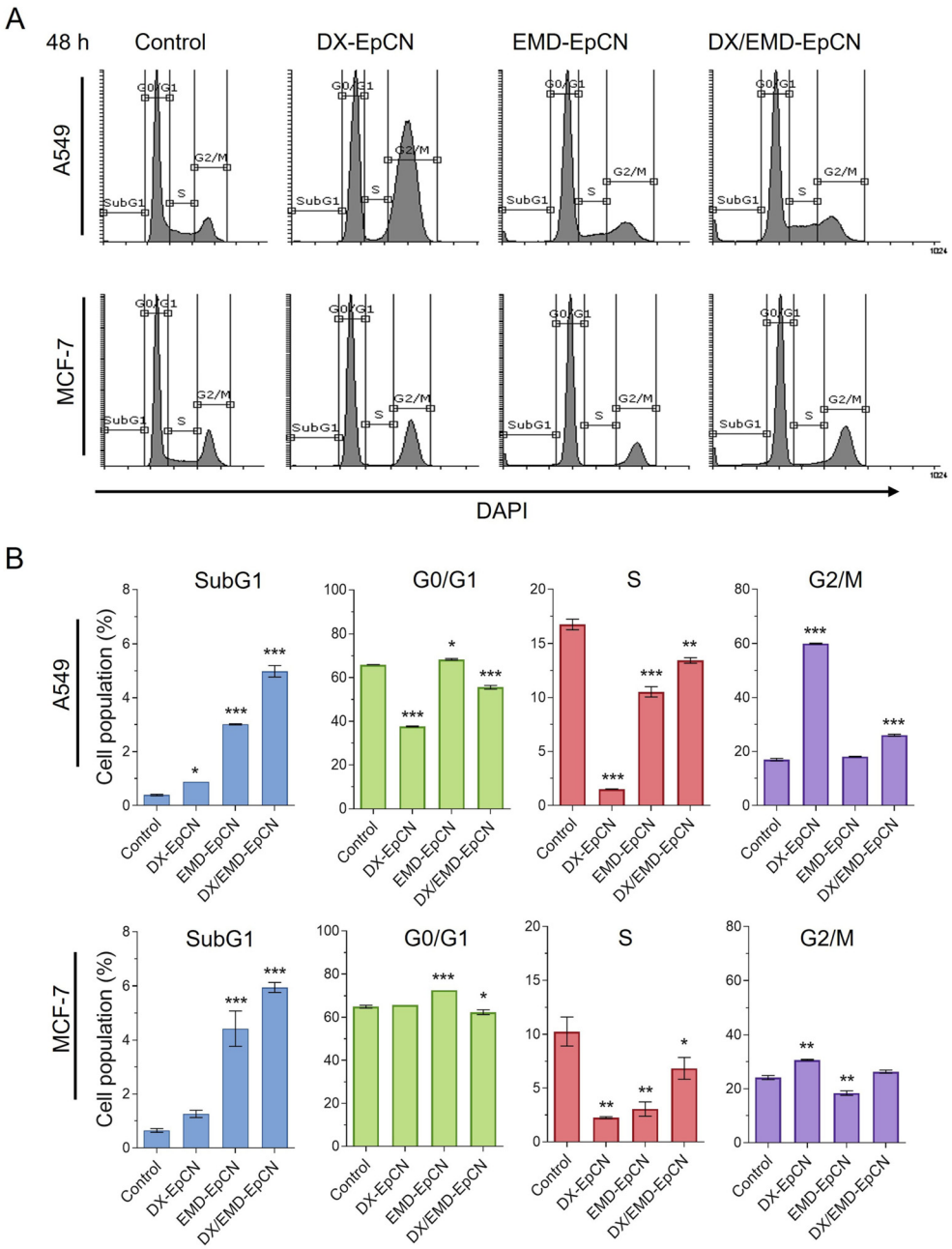

Fig. 8 Effect of drug-loaded EpCNs on cell cycle distribution in A549 and MCF-7 cells. (A) Histograms display DNA content of A549 and MCF-7 cells after 48 h of treatment with DX-EpCN, EMD-EpCN, or DX/EMD-EpCN. DAPI staining and flow cytometry were performed to detect the cell cycle distribution. Untreated cells served as the control group. (B) Quantitative analysis of cell populations in SubG1, G0/G1, S, and G2/M phases. Data are presented as mean ± SD. *$p < 0.05$; **$p < 0.01$; **$p < 0.001$ compared to the untreated control group.

cycle progression, cell cycle of A549 and MCF-7 cells were evaluated by flow cytometry after treated with drug-loaded EpCNs (DX-EpCN, EMD-EpCN, and DX/EMD-EpCN) for 48 h. As shown in Fig. 8A and B, both single drug-loaded EpCN treatments (DX-EpCN and EMD-EpCN) resulted in significant alterations in cell cycle distribution when compared to untreated controls. DX-EpCN markedly increased the percentage of cells in the G2/M phase, from 17% (control) to 60% in A549 cells, and from 24% to 31% in MCF-7 cells. This observation aligns with DX mechanism that triggers G2/M arrest in response to DNA damage.[32]

c-Myc stimulates proliferation by inducing cells to exit the G0/G1 phase, promoting entry into the S phase, by activation of the transcription of CDKs, cyclins, E2F1, and/or inhibits the

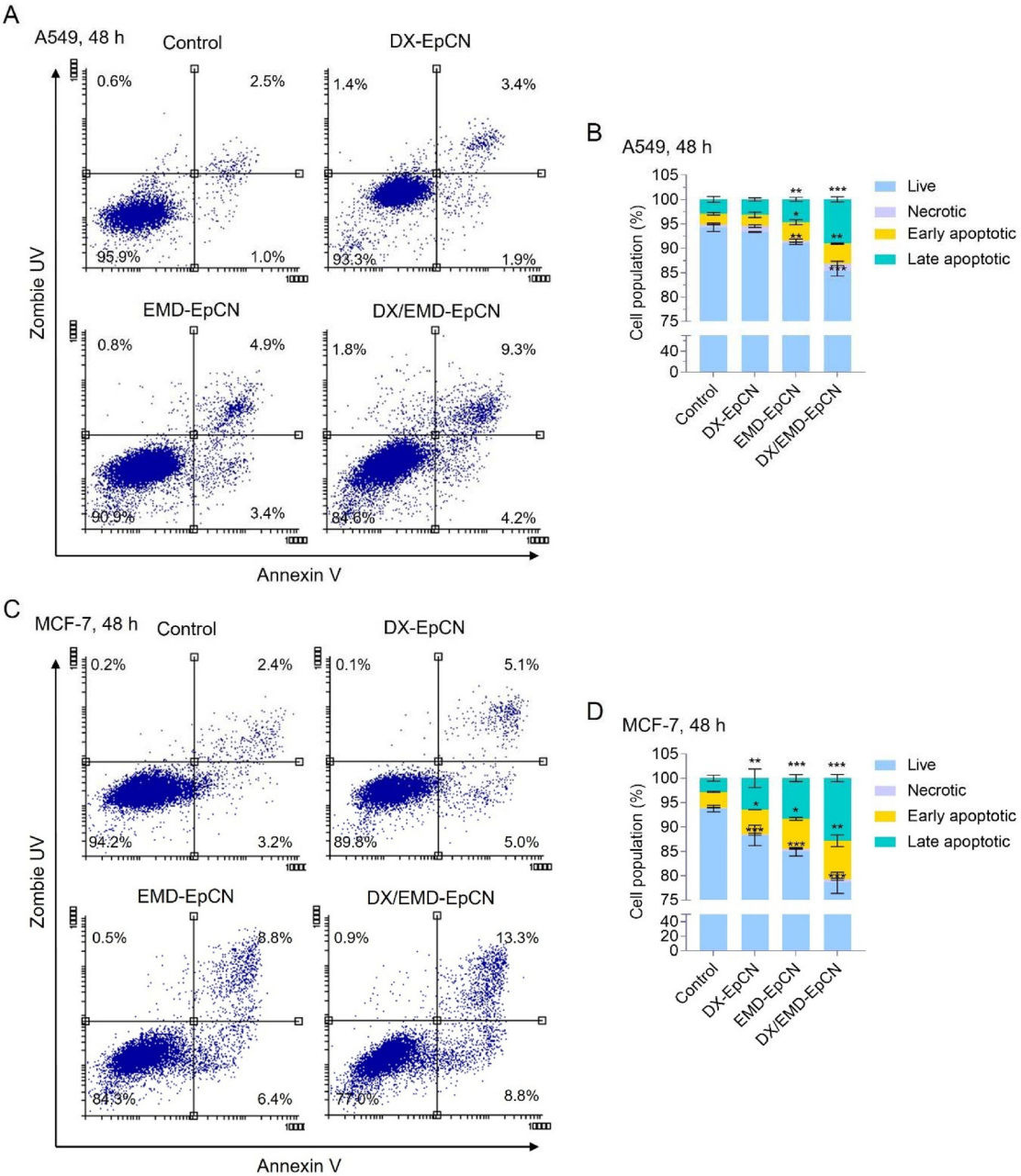

Fig. 9 The effect of drug-loaded EpCN formulations on apoptosis induction in A549 and MCF-7 cells. Apoptosis and necrosis were determined by annexin V/Zombie UV double staining followed by flow cytometry. (A and C) Representative results of dot plots from flow cytometry of A549 (A) and MCF-7 (C) cells after treatment with DX-EpCN, EMD-EpCN, or DX/EMD-EpCN for 48 h. Quadrants showing annexin V/Zombie UV fluorescence are numbered as follows: live (annexin V-/Zombie UV-), necrotic (annexin V-/Zombie UV+), Early apoptotic (annexin V+/Zombie UV-), and Late apoptotic (annexin V+/Zombie UV+) cells. (B and D) Quantification of percentage of cell population in different stages in A549 (B) and MCF-7 (D) cells. Data are presented as mean ± SD. *$p < 0.05$; **$p < 0.01$; **$p < 0.001$ *vs.* control or as indicated.

expression of CDK inhibitors.[33–35] EMD remarkably induced c-Myc degradation *via* a ubiquitin-proteasomal pathway,[9] which might influence the induction of the G0/G1 cell cycle arrest in cancer cells. G0/G1 phase cell cycle arrest associated with a decrease in the number of cells in the S and G2/M phases of the cell cycle. As expected, EMD-EpCN increased proportion of cells in the G0/G1 phase in both cell lines, from 66% to 69% in A549 cells and from 65% to 72% in MCF-7 cells (Fig. 8B). Although the proportion of cells in the S phase of A549 cells decreased from 17% to 10%, with no significant changes observed at the G2/M phase of the cell cycle. However, the number of cells at the S and G2/M phases of MCF-7 cells (EMD sensitive cells) decreased significantly after treatment with EMD-EpCN, from 10% to 3% and from 24% to 18%, respectively.

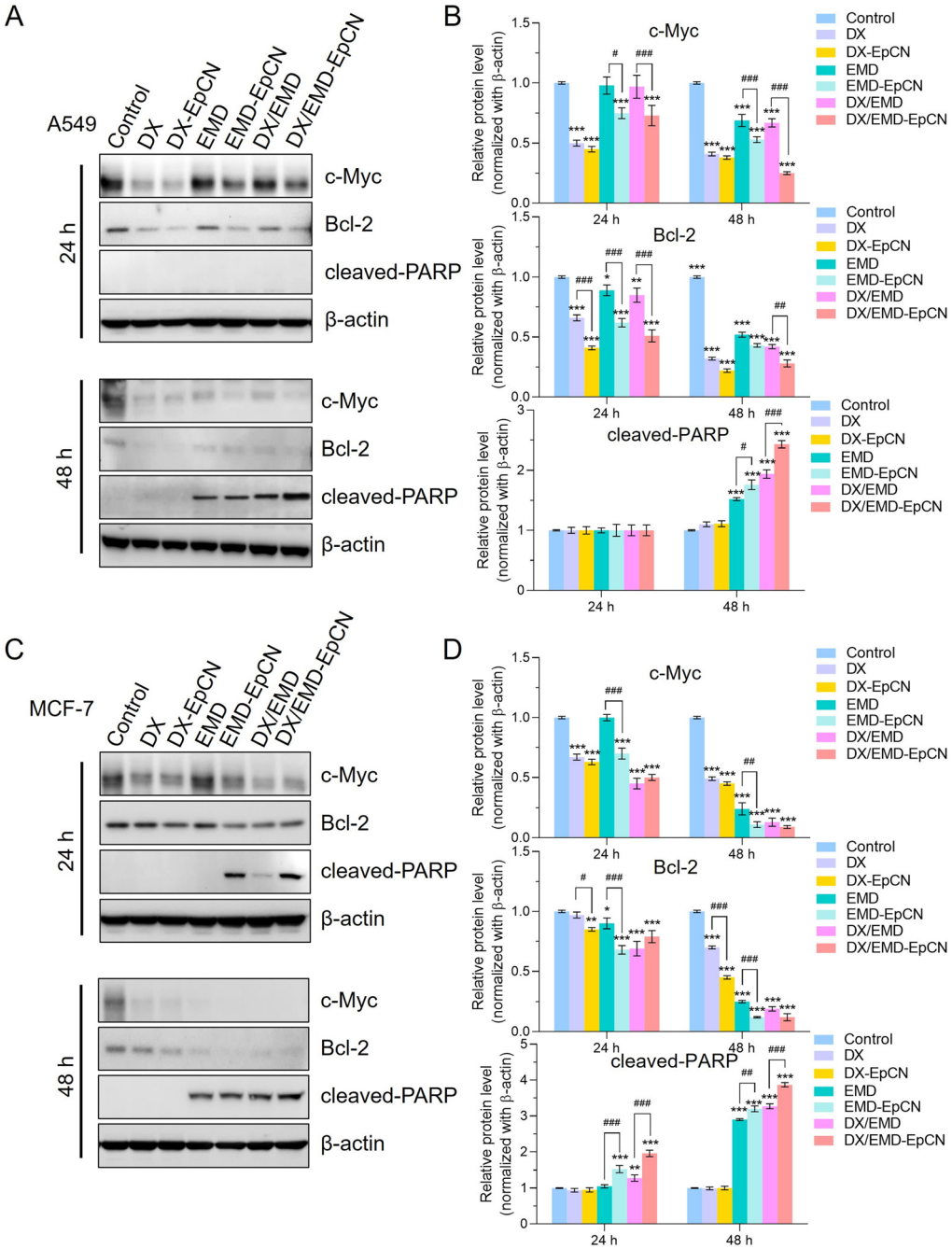

Fig. 10 Effects of drug-loaded EpCNs and their free drugs on the expression of c-Myc, Bcl-2, and cleaved-PARP in A549 and MCF-7 cells. (A and C) Representative western blot images showing protein expression levels of c-Myc, Bcl-2, and cleaved-PARP in A549 (A) and MCF-7 (C) cells after treatment with free drugs (DX, EMD, DX/EMD) and drug-loaded EpCNs (DX-EpCN, EMD-EpCN, DX/EMD-EpCN) for 24 and 48 h. β-actin was used as a loading control. (B and D) Quantitative analysis of relative protein expression levels normalized to β-actin in A549 (B) and MCF-7 (D) cells. Data are presented as mean ± SD. *$p < 0.05$; **$p < 0.01$; **$p < 0.001$ *vs.* control or as indicated; #$p < 0.05$; ##$p < 0.01$; ###$p < 0.001$ between treatment groups.

Since cleavage of chromosomal DNA into oligonucleosomal size fragments is a biochemical hallmark of apoptosis,[36] which can be detected as an increase in the number of cells at SubG1 phase. We found that DX/EMD-EpCN treatment dramatically increases the SubG1 population compared to both single drug-loaded EpCNs (Fig. 8B). The results indicated that combination therapy may enhance the induction of apoptosis in cancer cells more effectively than either treatment alone. DX/EMD-EpCN also promoted cell accumulation in both G0/G1 and G2/M phases in A549 and MCF-7 cells, indicating that simultaneous targeting with multiple checkpoints contributed to provide a more effective growth arrest.

Having demonstrated that DX/EMD-EpCN induced multiphase cell cycle arrest in both A549 and MCF-7 cells, specifically inducing SubG1 arrest (apoptosis indicator) compared to both single drug-loaded EpCNs. To confirm whether DX/EMD-EpCN induces cell death through the apoptosis pathway, we performed annexin V/Zombie UV staining in A549 and MCF-7 cells after 48 h treatment with DX-EpCN, EMD-EpCN or DX/EMD-EpCN. Annexin V interacts with phosphatidylserine on the surface of early apoptotic cells,[37] whereas Zombie UV, a viability dye that reacts with amines, enters cells with damaged membranes, indicating late apoptotic or dead cells. As expected, DX/EMD-EpCN was able to effectively induce apoptosis in both A549 and MCF-7 cells compared to both single drug-loaded EpCNs (Fig. 9A and C). In A549 cells, the percentage of cells following apoptosis after treatment with DX/EMD-EpCN was 13.1% (early apoptosis + late apoptosis), whereas treatment with DX-EpCN and EMD-EpCN resulted in 5.4% and 8.4% of apoptotic cells, respectively (Fig. 9B). Similarly, in MCF-7 cells, the percentage of apoptotic cells was 20.7% in the DX/EMD-EpCN treatment, while treatment with DX-EpCN and EMD-EpCN showed a 11.4% and a 14.4% of apoptotic cells, respectively (Fig. 9D). Notably, while EMD-EpCN by itself showed a modest pro-apoptotic effect, the combination with DX largely increased the apoptosis rate in both A549 and MCF-7 cells, hence indicating a synergistic interaction between the two drugs. Moreover, the percentage of necrotic cells was consistently low, remaining below 2% in A549 cells and below 1% in MCF-7 cells across all treatments. Thus, drug-loaded EpCNs appear to induce cell death predominantly *via* apoptotic mechanisms rather than necrosis. These results indicated that DX/EMD-EpCN effectively inhibited the proliferation of A549 and MCF-7 cells by disrupting cell cycle progression and inducing apoptosis.

3.7. DX/EMD-EpCN modulates c-Myc, Bcl-2, and cleaved-PARP expression to promote apoptosis

To gain a better understanding of the molecular mechanisms underlying the synergism of DX/EMD-EpCN, we determined the expression of apoptosis-related proteins, including c-Myc, Bcl-2, and cleaved-PARP, using western blotting (Fig. 10A–D). We found that EMD and EMD-EpCN significantly reduced c-Myc expression in both A549 and MCF-7 cells with a time-dependent manner (Fig. 10A and D), consistent with the role of EMD in promoting the degradation of c-Myc.[9] In both cell lines, DX/EMD-EpCN treatment shows the largest reduction in c-Myc levels when compared to EMD-EpCN after treatment for 48 h (Fig. 10C and D), hence synergistically inhibiting c-Myc expression.

Several studies indicate that Bcl-2 plays a crucial role in the survival of cancer cells by interacting with pro-apoptotic proteins, thereby preventing mitochondrial outer membrane permeabilization and the activation of cytotoxic caspases.[38] Fig. 10A and C show that DX/EMD-EpCN treatment significantly downregulated the anti-apoptotic protein Bcl-2 in both cell lines in a time-dependent manner. This reduction in Bcl-2 suggests that DX/EMD-EpCN shifts the balance towards pro-apoptotic signaling. Poly (ADP-ribose) polymerase (PARP) is a protein that is specifically targeted for proteolytic cleavage during apoptosis. Its cleavage has been widely used as a marker for apoptosis.[39] As shown in Fig. 10A and C, at 48 h, DX/EMD-EpCN treatment significant increased cleaved-PARP level higher than that free drug combinations (DX/EMD) or single drug-loaded EpCNs treatments in both A549 and MCF-7 cells. Although there was a significant decrease in c-Myc and Bcl-2 levels after treatment with DX-EpCN, this treatment failed to induce cell death in A549 cells, as indicated by the absence of the apoptosis marker cleaved-PARP (Fig. 10A and B) and the absence of subG1 population in the cell cycle (Fig. 8B), indicate the limitations of single drug treatment, as the downregulation of survival proteins alone is insufficient to activate apoptotic pathways.

In summary, cell cycle analysis, annexin V/Zombie UV staining, and western blotting results indicate that the increased cytotoxicity and apoptosis induced by DX/EMD-EpCN were mediated by suppression of proliferative signaling *via* c-Myc degradation, inhibition of anti-apoptotic defence through Bcl-2 downregulation, and activation of apoptosis, as evidenced by elevated levels of cleaved-PARP. Together, these results indicate that the DX/EMD-EpCN effectively modulates key molecular targets involved in both cell survival and cell death, thereby providing a clearer mechanistic basis for the observed synergistic anticancer effects.

4. Conclusions

In this study, a co-delivery of DX and EMD by EpCN to improve anticancer efficacy *via* combination therapy was demonstrated. EMD was encapsulated in hydrophobic sites of the cyclodextrins while DX was loaded in hydrophilic regions of the EpCN. The EpCNs were synthesized through the crosslinking of β-cyclodextrin with epichlorohydrin and characterized by DLS, AFM, SEM, and NMR to confirm their nanoscale size, positive surface charge, and drug loading and locate in the EpCNs. DX/EMD-EpCN exhibited pH-sensitive release characteristics, enabling accelerated drug release under acidic conditions that mimic tumour microenvironment. The SRB assay indicated that the dual drug-loaded EpCN (DX/EMD-EpCN) exhibited enhanced cytotoxicity relative to both single-drug loaded EpCNs and free drug combination. The dual-drug EpCN

demonstrated a reduced IC_{50} values, an increased dose-reduction index, with a significant synergy (CI < 0.6) in both A549 and MCF-7 cell lines. Studies on cellular uptake demonstrated a selective accumulation of DX/EMD-EpCN in cancer cells, while normal fibroblasts exhibited a minimal uptake. Additionally, DX/EMD-EpCN caused multi-phase cell cycle arrest and markedly enhanced apoptosis, as evidenced by annexin V/Zombie UV staining and increased level of cleaved-PARP. Western blot analysis revealed a significant reduction of c-Myc and Bcl-2 expression, together with a notable upregulation of cleaved-PARP, suggesting an activation of intrinsic apoptotic pathways, as summarized in Scheme 2. In conclusion, the nanosponge-based co-delivery provides a viable approach to enhance combination chemotherapy through an improved anticancer efficacy and a minimized off-target toxicity. The nanosponges provide a means to simultaneous encapsulate of hydrophilic and hydrophobic drugs in a single CN promoting a combined action of EMD and DX leading to cancer cell apoptosis.

Author contributions

Sunisa Thongsom: writing – original draft, writing – review & editing, methodology, investigation, data curation, conceptualization. Paolo Di Gianvincenzo: writing – original draft, writing – review & editing, methodology, investigation, data curation. Giulia Ciattaglia: investigation, formal analysis. Ahmed Subrati: writing – original draft, investigation, data curation. Desiré DiSilvio: investigation, data curation. Ariadna M. Birocco: investigation. Marco D'Abramo: supervision, resources. Chanchai Boonla: writing – review & editing, supervision. Pithi Chanvorachote: supervision, resources. Sergio E. Moya: writing – original draft, writing – review & editing, conceptualization, funding acquisition, project administration, supervision.

Conflicts of interest

There are no conflicts to declare.

Data availability

Data for this article, including dynamic light scattering readouts, fluorescence readouts, UV readouts, flow cytometry readouts, western blot full membrane images, scanning electron microscopy micrographs, and atomic force microscopy micrographs are available at Zenodo at https://zenodo.org/records/15852652.

Supplementary information: NMR spectra. See DOI: https://doi.org/10.1039/d5pm00183h.

Acknowledgements

S. E. M thanks the PID2020-114356RB-I00 project from the Ministry of Science and Innovation of the Government of Spain and the Maria de Maeztu Units of Excellence Program from the Spanish State Research Agency – Grant no. MDM-2017-0720.

References

1 R. L. Siegel, A. N. Giaquinto and A. Jemal, *Ca-Cancer J. Clin.*, 2024, **74**, 12–49.
2 K. Cheung-Ong, G. Giaever and C. Nislow, *Chem. Biol.*, 2013, **20**, 648–659.
3 M. S. Ricci and W. X. Zong, *Oncologist*, 2006, **11**, 342–357.
4 D. M. Evans, J. Fang, T. Silvers, R. Delosh, J. Laudeman, C. Ogle, R. Reinhart, M. Selby, L. Bowles, J. Connelly, E. Harris, J. Krushkal, L. Rubinstein, J. H. Doroshow and B. A. Teicher, *Cancer Chemother. Pharmacol.*, 2019, **84**, 359–371.
5 R. Ludwig and D. S. Alberts, *Cancer Chemother. Pharmacol.*, 1984, **12**, 142–145.
6 A. Pearce, M. Haas, R. Viney, S. A. Pearson, P. Haywood, C. Brown and R. Ward, *PLoS One*, 2017, **12**, e0184360.
7 R. Bayat Mokhtari, T. S. Homayouni, N. Baluch, E. Morgatskaya, S. Kumar, B. Das and H. Yeger, *Oncotarget*, 2017, **8**, 38022–38043.
8 M. Kciuk, A. Gielecińska, S. Mujwar, D. Kołat, Ż Kałuzińska-Kołat, I. Celik and R. Kontek, *Cells*, 2023, **12**, 659.
9 N. Sriratanasak, K. Petsri, A. Laobuthee, W. Wattanathana, C. Vinayanuwattikun, S. Luanpitpong and P. Chanvorachote, *Mol. Pharmacol.*, 2020, **98**, 130–142.
10 N. Suetrong, K. Chansaenpak, S. Impeng, P. Pinyou, V. Blay, R. Blay-Roger, S. Lisnund, P. Kanjanaboos, Y. Hanlumyuang, S. Wannapaiboon and W. Wattanathana, *Crystals*, 2021, **11**, 979.
11 P. Chanvorachote, N. Sriratanasak and N. Nonpanya, *Anticancer Res.*, 2020, **40**, 609.
12 G. Donati and B. Amati, *Mol. Oncol.*, 2022, **16**, 3828–3854.
13 A. P. Sherje, B. R. Dravyakar, D. Kadam and M. Jadhav, *Carbohydr. Polym.*, 2017, **173**, 37–49.
14 A. P. Sherje, A. Surve and P. Shende, *J. Mater. Sci.:Mater. Med.*, 2019, **30**, 74.
15 G. Utzeri, P. M. C. Matias, D. Murtinho and A. J. M. Valente, *Front. Chem.*, 2022, **10**, 2022.
16 S. Thongsom, P. Di Gianvincenzo, S. Konkankun, A. Blachman, S. Bongiovanni Abel, N. Madared, C. Boonla, P. Chanvorachote and S. E. Moya, *Colloid Interface Sci. Commun.*, 2024, **62**, 100803.
17 X. Liu, W. Li and G. Xuan, *IOP Conf. Ser.:Mater. Sci. Eng.*, 2020, **774**, 012108.
18 A. Phungula, S. Zuffi, S. Thongsom, P. Di Gianvincenzo, S. G. Reyes, A. B. Caribé Dos Santos Valle, F. Pittella, F. Albericio, B. G. de la Torre and S. E. Moya, *Nanoscale*, 2025, **17**, 4659–4669.
19 L. Desiderio, N. S. Gjerde, E. Tasca, L. Galantini, I. Llarena, P. Di Gianvincenzo, S. Thongsom, S. E. Moya and M. Giustini, *J. Colloid Interface Sci.*, 2024, **664**, 972–979.

20 S. Thongsom, W. Suginta, K. J. Lee, H. Choe and C. Talabnin, *Apoptosis*, 2017, **22**, 1473–1484.
21 T. C. Chou and N. Martin, *CompuSyn software*, ComboSyn Inc., Paramus, NJ, 2005.
22 T. C. Chou, *Cancer Res.*, 2010, **70**, 440–446.
23 Y.-H. Wen, P.-I. Hsieh, H.-C. Chiu, C.-W. Chiang, C.-L. Lo and Y.-T. Chiang, *Mater. Today Bio*, 2022, **17**, 100482.
24 N. Deirram, C. Zhang, S. S. Kermaniyan, A. P. R. Johnston and G. K. Such, *Macromol. Rapid Commun.*, 2019, **40**, 1800917.
25 P. Yadav, J. Jain and A. P. Sherje, *React. Funct. Polym.*, 2021, **165**, 104970.
26 J. Shi, Y. Ren, J. Ma, X. Luo, J. Li, Y. Wu, H. Gu, C. Fu, Z. Cao and J. Zhang, *J. Nanobiotechnol.*, 2021, **19**, 188.
27 S. Chouaib, M. Z. Noman, K. Kosmatopoulos and M. A. Curran, *Oncogene*, 2017, **36**, 439–445.
28 S. Swaminathan, L. Pastero, L. Serpe, F. Trotta, P. Vavia, D. Aquilano, M. Trotta, G. Zara and R. Cavalli, *Eur. J. Pharm. Biopharm.*, 2010, **74**, 193–201.
29 F. Trotta, D. Chiara, C. Fabrizio, M. Barbara and R. Cavalli, *Expert Opin. Drug Delivery*, 2014, **11**, 931–941.
30 E. Blanco, H. Shen and M. Ferrari, *Nat. Biotechnol.*, 2015, **33**, 941–951.
31 K. Vermeulen, D. R. Van Bockstaele and Z. N. Berneman, *Cell Proliferation*, 2003, **36**, 131–149.
32 G. Minotti, P. Menna, E. Salvatorelli, G. Cairo and L. Gianni, *Pharmacol. Rev.*, 2004, **56**, 185–229.
33 A. Baluapuri, E. Wolf and M. Eilers, *Nat. Rev. Mol. Cell Biol.*, 2020, **21**, 255–267.
34 W. W. Marhin, S. Chen, L. M. Facchini, A. J. Fornace Jr and L. Z. Penn, *Oncogene*, 1997, **14**, 2825–2834.
35 Z. E. Stine, Z. E. Walton, B. J. Altman, A. L. Hsieh and C. V. Dang, *Cancer Discovery*, 2015, **5**, 1024–1039.
36 J. H. Zhang and M. Xu, *Cell Res.*, 2000, **10**, 205–211.
37 I. Vermes, C. Haanen, H. Steffens-Nakken and C. Reutellingsperger, *J. Immunol. Methods*, 1995, **184**, 39–51.
38 F. Braun, D. C. T. Sophie, B.-C. Joséphine and P. Juin, *Cell Cycle*, 2013, **12**, 2937–2947.
39 F. J. Oliver, G. de la Rubia, V. Rolli, M. C. Ruiz-Ruiz, G. de Murcia and J. M.-D. Murcia, *J. Biol. Chem.*, 1998, **273**, 33533–33539.